Impact of National Development Policies on Agricultural Land Use Dynamics in Chichaoua, Morocco: A Two-Decade Remote Sensing Analysis

Ikram El Hazdour, Michel Le Page, Lionel Jarlan, Marielle Montginoul, Lahoucine Hanich

Remote Sensing Applications: Society and Environment 42 (2026) 102034

Contents lists available at ScienceDirect

Remote Sensing Applications: Society and Environment

journal homepage: www.elsevier.com/locate/rsase

Impact of National Development Policies on Agricultural Land Use Dynamics in Chichaoua, Morocco: A Two-Decade Remote Sensing Analysis

Ikram El Hazdour [a,b,*], Michel Le Page [a], Lionel Jarlan [a], Marielle Montginoul [c], Lahoucine Hanich [b,d]

[a] Univ Toulouse, CNES, CNRS, INRAE, IRD, CESBIO, Toulouse, France
[b] L3G Laboratory, Faculty of Sciences and Techniques, Cadi Ayyad University, Marrakech, Morocco
[c] G-EAU, Univ Montpellier, AgroParisTech, BRGM, CIRAD, INRAE, Institut Agro, IRD, Montpellier, France
[d] Mohammed VI Polytechnic University (UM6P), Geology and Sustainable Mining Institute (GSMI), Morocco

ARTICLE INFO

Dataset link: GEE LULC Classification code and dataset (Original data)

Keywords:
LULC
Random-forest
Classification
Remote-sensing
GEE
National-policies

ABSTRACT

Agricultural development policies can boost productivity and profits but also lead to adverse consequences when natural resources are exploited unsustainably, particularly in systems vulnerable to drought and climate change.

This study provides a novel, comparative upstream-downstream assessment of land-use evolution in Morocco's semi-arid Chichaoua region under national development policies, particularly the Green Moroccan Plan, by integrating multi-source remote sensing. Chichaoua offers a peculiar case where newly-cultivated land upstream of a historic irrigated area facilitates a straightforward evaluation of policy-related land and water use changes. The upstream zone, previously unexploited, relies on boreholes, whereas the downstream area has historically depended on natural springs for traditional irrigation. Utilising Sentinel-2 and Landsat imagery and ground data from 2023, a Random Forest model was employed for crop-classification over 23-years (~2000-2023), and land-use transitions were analysed through transition matrices. Total irrigated area doubled, increasing from ~2871 to ~6569 ha, but with stark contrasts between the zones.

Upstream areas expanded by +4000 ha, featuring 22% cash-crops and 41% olive trees, while downstream zones witnessed a 40% decline in olive cultivation. National policies offering grants and improving land and water access are correlated with shifts toward cash-crop-focused farming upstream, potentially fuelling productivity gains. However, this transformation appears to be associated with reduced natural spring availability, potentially undermining traditional downstream agriculture. This dual impact highlights both the benefits of increased agricultural productivity and the challenges of resource depletion and threats to traditional farming. The findings reveal critical trade-offs between agricultural gains and environmental risks in vulnerable regions.

* Corresponding author. Univ Toulouse, CNES, CNRS, INRAE, IRD, CESBIO, Toulouse, France.
E-mail address: ikram.el_hazdour@ird.fr (I. El Hazdour).

https://doi.org/10.1016/j.rsase.2026.102034
Received 26 February 2025; Received in revised form 23 March 2026; Accepted 20 April 2026
Available online 21 April 2026

1. Introduction

Land Use/Land Cover (LULC) changes constitute a complex process with consequences for many ecosystems (Irwin and Geoghegan, 2001; Lambin and Geist, 2006; Tayyebi et al., 2014; Das and Das, 2024; Kanji and Das, 2025). These transformations, whether they be as a consequence of urbanisation (Das and Das, 2022) or agricultural intensification, provide critical insights into human-environment interactions (Mukherjee et al., 2024).

Of these transformations, agricultural land use changes, in particular, have a significant effect on the water cycle and water resources. Groundwater depletion is most pronounced in regions of intensive agricultural land use, especially in semi-arid and arid areas, where low recharge rates and surface water scarcity exacerbate the issue (Siebert et al., 2010; Rodell et al., 2018; Famiglietti and Ferguson, 2021; Scanlon et al., 2023). Notably, major global food-producing regions like California's Central Valley, the Central US, Northern India, Pakistan, and the North China Plain, have witnessed elevated levels of overexploitation rates of non-renewable aquifers for irrigation purposes (Wada et al., 2012; Dalin et al., 2017; Davis et al., 2019). This global challenge of groundwater overexploitation is driven by a complex set of factors.

The aforementioned changes are driven by a multitude of interconnected factors, including, but not limited to, environmental factors (e.g., climate change (Wang et al., 2020) and extreme weather events), demographic factors (e.g., population growth and urbanisation), economic factors (e.g., commercial agricultural intensification (Lambin et al., 2001)), and policy-related factors (e.g., land tenure regime (Ostrom et al., 1999) or crop subsidies (Elfert and Bormann, 2010)). In recent decades, the influence of global economic forces among these drivers has become increasingly prominent.

Indeed, land use changes have been predominantly shaped by demands for export-oriented production, influenced by globalisation, rising incomes, and trade (Liu et al., 2013). In California's Central Valley, for instance, transitions towards high-revenue perennial crops such as vineyards and orchards – spurred by market demands, price fluctuations, revenue potential, and consumer preferences – have led to excessive groundwater overdraft during drought periods (Faunt et al., 2016; Mall and Herman, 2019; Gebremichael et al., 2021). These market-driven shifts are often directly exacerbated by policy interventions.

Policy measures, particularly subsidies, further amplify these dynamics and can exacerbate resource depletion. Subsidised water and energy tariffs for agriculture, aimed at boosting productivity and food security, often drive shifts to water-intensive crops, leading to groundwater overextraction (Moor et al., 1997; Turner et al., 2004). It was, for instance, the case in India, during the Green Revolution, wherein the government provided financial incentives for the cultivation of high-yield crops (e.g., rice, wheat, and sugarcane), irrigation infrastructure, and electricity for tube wells. Whilst the implementation of this policy has improved food security and farmer incomes; it has also been associated with a widespread of groundwater depletion and widened disparities (Sidhu et al., 2020; Chatterjee et al., 2024). Similar policy-linked dynamics have been documented in Saudi Arabia by Li et al. (2023); who quantified field acreages and numbers and found that agricultural subsidies initially led to agricultural expansion (e.g., wheat production) at the cost of non-renewable water resources, while later subsidy removals led farmers to adopt even more water-intensive fodder crops. Such cases reinforce the need for robust monitoring of policy impacts on land use, particularly in regions characterised by diverse and evolving agricultural landscapes.

Understanding the repercussions of development policies on land use changes is crucial, especially in regions where various agricultural practices coexist; and such regions necessitate comprehensive, fine-scale mapping and monitoring to accurately track these dynamics. These regions frequently feature a mix of small-scale, traditional irrigation plots alongside large-scale, modern agricultural systems. The issue has become increasingly critical in Morocco - which is the focus of this study - where severe recent droughts (Oukaddour et al., 2024) and a generalisation of intensive groundwater-based farming have heightened pressure on water resources. To address this, our study aims to quantify agricultural land use change in a data-scarce region of Morocco and assess its potential association with national development plans using a reproducible remote sensing framework. The effective monitoring of such changes at a fine scale is facilitated by remote sensing, which provides a powerful and well-established toolkit.

To quantify such changes, remote sensing imagery has played a pivotal role in crop classification and LULC monitoring over the decades. Recent reviews have highlighted significant advancements in this area (Gómez et al., 2016; Ma et al., 2017; Phiri and Morgenroth, 2017; Talukdar et al., 2020; Hermosilla et al., 2022). Among the available datasets, the Landsat archive has provided a window into the past and has enabled retrospective monitoring of global land cover and ecological shifts over time (Wulder et al., 2012; Roy et al., 2014). In particular, the improved Landsat Collection 2 dataset – with its robust atmospheric corrections and standardised processing – is now mostly used for mapping and monitoring LULC changes (Crawford et al., 2023). While high-resolution datasets, such as SPOT (6-20m) (Disperati and Virdis, 2015) offer greater spatial detail, the data costs and the absence of a systematic archival collection has contributed to their limited uptake over the previous two decades (Wulder et al., 2018). Meanwhile, coarser datasets like MODIS (250-500 m) and VIIRS provide near-daily coverage but lack fine-scale resolution (Xin et al., 2013; Wan et al., 2015). Sentinel-2 (10 m, 4-16 day revisits) (European Space Agency), however, has provided a consistent dataset and has been widely applied in various applications (e.g., urbanization mapping (Furberg et al., 2019), wet grassland mapping (Rapinel et al., 2019), small scale agricultural crop mapping (Lambert et al., 2018), etc.). Combining Sentinel-2 and Landsat is particularly effective, especially for historical analyses at the plot-scale, as it leverages the strengths of both datasets. The analysis of these vast satellite datasets has been revolutionised by advances in machine learning and computing.

To process and classify these datasets, Machine Learning (ML) has been widely applied for LULC classification with supervised techniques demonstrating strong performance in classifying crops using satellite imagery (Zhao et al., 2020; Alami Machichi et al., 2023)<b.> Among these, Random Forest (RF) (Breiman, 2001) is one of the classifiers that has been widely used for LULC classification using remote-sensing data (Pal, 2005; Sheykhmousa et al., 2020). RF has proven particularly effective due to its low sensitivity to overfitting and computational efficiency when handling large; complex datasets (Belgiu and Drăguţ, 2016), making it

well-suited for long term classification purposes (this study). The advent of cloud-based computing systems (Yang et al., 2017) such as Google Earth Engine (GEE) (Gorelick et al., 2017) has revolutionised this field by providing: (a) computational power to handle complex landscapes (Kelley et al., 2018); (b) diverse ML classifiers for large-scale analysis (Shelestov et al., 2017; Teluguntla et al., 2018), (c) multi-sensor integration capabilities through its extensive data collections (Sujud et al., 2021; Guo et al., 2022); and (d) efficient temporal data aggregation (Carrasco et al., 2019; Phan et al., 2020). For this study, GEE's capabilities were essential to address the challenge of long-term land use classification, enabling efficient processing of multi-decadal satellite data while minimising computational constraints. This technical capacity facilitates the addressing of a critical research gap concerning the impact of agricultural policies in understudied regions.

In summary, the rationale for this study is threefold. First, it is imperative to comprehend the unintended environmental consequences of agricultural development policies, an issue well-documented globally but underexplored in the specific context of Morocco. Second, quantifying these policy impacts requires robust, long-term, and fine-scale monitoring of agricultural land use, which is particularly challenging in data-scarce regions with heterogeneous farming systems. Third, leveraging the multi-source remote sensing within a cloud-computing environment and a trainable RF model in this study would provide a reproducible methodological framework to overcome these challenges. Guided by this rationale, this paper aims to address two key scientific challenges: (1) quantifying historical agricultural land use changes and analysing their relationship with agricultural development policies in Morocco's semi-arid Chichaoua region (Tensift basin) - where national development plans have been a major factor in the expansion of intensive agriculture, yet their unintended effects on environmental sustainability and resilience of farming systems remain undocumented; and (2) addressing a methodological gap in contexts where data is scarce by using a reproducible framework that relies on model retraining for long-term monitoring using limited ground data. This will help to fill the knowledge gap regarding understudied agro-systems.

This study, therefore, provides a novel, policy-explicit quantification of agricultural land use change by leveraging a reproducible, long-term remote sensing framework, to explore its association with successive national development plans in a data-scarce, heterogeneous agricultural region of Morocco.

To achieve this, this observational study is structured around three research questions:

RQ1: What are the distinct, 23-year trajectories of irrigated land in the upstream and downstream zones of the Chichaoua region, specifically identifying the 2010 breakpoint?
RQ2: Which crop groups are primarily responsible for the observed expansion and contraction of agricultural land at the regional level?
RQ3: How can these trends be framed within the interplay of national development policies, such as the Green Moroccan Plan, and concurrent climate variability?

The paper is structured as follows: Section 2 offers an overview of the Moroccan agricultural development plans. Section 3 details the materials and methods used, including the study area's context, and the land use classification workflow. Section 4 presents the results, with the first part focusing on the accuracy of the methods; and the second part examining the evolution of land use. Section 5 provides a discussion interpreting the dynamics behind the previously observed temporal pattern, exploring the potential role of national policies in the observed land use changes and their progression over time, and addressing the study's limitations.

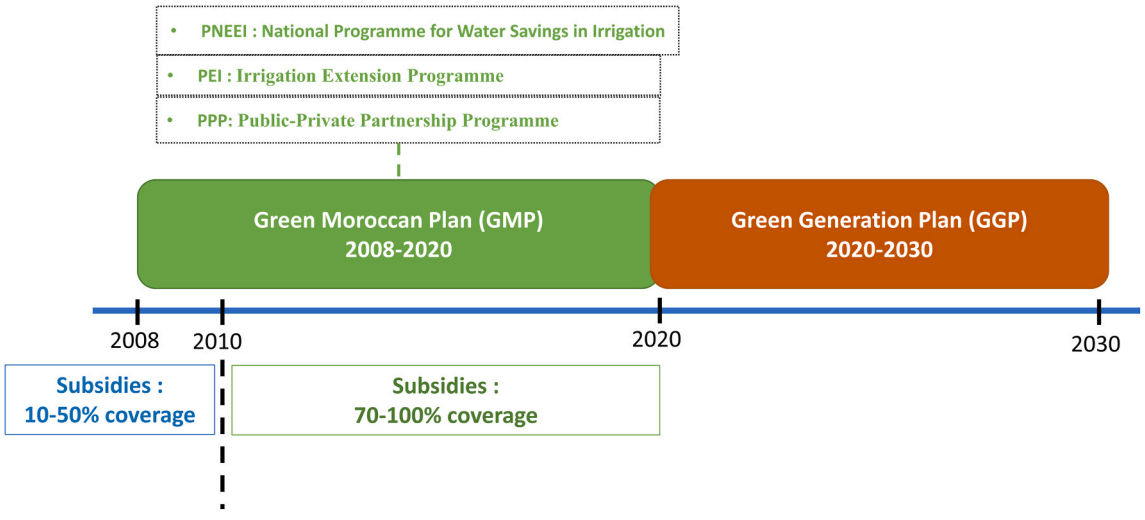

Fig. 1. A schematic summary of the main agricultural development policy framework. This timeline highlights the transition to high-subsidy regimes (70-100%) that funded the orchard expansion and borehole intensification observed in the results.

2. A national agricultural development policy linked to land use changes and irrigation expansion

As Morocco faces a semi-arid (and arid) climate, irrigation constitutes an important component of rural economic activities and represents 50% of agricultural added value, with groundwater accounting for 40% of these irrigated lands (Molle and Tanouti, 2017). Morocco's agriculture sector (renowned for producing citrus fruits, tomatoes, olives, sugar, dates, and argan) plays a crucial role in driving the nation's economy, representing 12.3% of GDP and supported by 30.4 million hectares of fertile land and 1.6 million farmers.

Like many countries where agriculture constitutes the primary economic activity, Morocco has adopted development strategies in order to boost agricultural productivity and modernise its agricultural sector. The government allocates 3.4 billion MAD annually (330 million euros) – approximately 0.29% of GDP – to agricultural aid and subsidies, with spending on the sector rising 36% since 2011. Over half of the investment supports irrigation, with the rest directed towards equipment, livestock, and fruit tree planting (Amachraa & MAAD, 2023).

The implementation of several development plans, particularly the Green Moroccan Plan (GMP) (2008-2020) and its associated project, the National Programme for Water Savings in Irrigation (PNEEI), along with its successor, the Green Generation Plan (GGP) (2020-2030), has facilitated better access to land, water, and subsidies. A schematic overview of this policy chronology is presented in Fig. 1. The GMP aimed to transform agriculture into a specific and consistent agro-industry, prioritising the production of high-value-added (cash-crops) products to drive economic growth and enhance food security. It prioritised irrigation improvements, market modernization, and partnerships with stakeholders (ADA, n.d). The GMP's two pillars focused on export-oriented agriculture and reducing rural poverty through “reconversion” projects (promoting arboriculture instead of cereals), diversification projects (promoting local production), and intensification projects (improving yields through technical support) (Mahdi, 2014; Mathez and Loftus, 2023). Its successor (the GGP) emphasises job creation, sustainable resource use, youth engagement, cooperative development, and addressing value chain gaps to promote sustainable growth.

Subsidising agriculture and irrigation were central to these plans. GMP, for example, received 104 billion Dirhams in investments between 2008 and 2018, 60% of which were injected by the private sector, according to the Department of Agriculture. Prior to GMP, agricultural subsidies ranged from only 10% to 30% and covered irrigation infrastructure costs, soil erosion control, and land preparation, as outlined in the 1985 official gazette (number 3773). However, following GMP's implementation (2008-2010), subsidies significantly increased, covering 80% for localised irrigation projects undertaken individually, and up to 100% for collective irrigation projects or those implemented by small-scale farmers, with incentives encouraging collective irrigation systems, as outlined in the 2010 official gazette (number 5818). Additional support was provided for land improvement at 30%, rainwater harvesting at 50%, irrigation complement projects (e.g., well digging, pumping equipment, water tank development) at 50%, and tree planting at 80% for certified olive and almond seedlings, as well as planting materials for trees like fig, carob, pistachio, walnut, pomegranate, cherry, and medlar, when purchased from state-approved nurseries in areas not covered by state planting programs. In 2011, grants were revised according to the Official Gazette of 2011 (Number 5914), increasing support to 70%-80% for irrigation complement projects and well and borehole digging, which were previously covered at only 50%, with full coverage provided for the supply and installation of irrigation systems. For further details, the Official Gazettes can be accessed on the General Government Secretariat website (http://www.sgg.gov.ma/Accueil.aspxwebsite).

Water management, land tenure restructuring, and agricultural value chain management were central elements of the development strategies.

Water management is a critical challenge in the country's arid context, necessitating improved efficiency in irrigated agriculture. To address this, three key programmes were implemented under which some of the subsidies discussed above were offered: the National Irrigation Water-Saving Programme (PNEEI), the Irrigation Extension Programme (PEI), and the Public-Private Partnership programme (PPP). The PNEEI focused on promoting the widespread adoption of drip irrigation over traditional gravity irrigation, as a means of conserving irrigation water. The PEI aimed to expand irrigated agriculture by developing new perimeters. Meanwhile, the PPP in irrigation focused on enhancing the management of irrigation water and conserving groundwater by utilising non-conventional water sources through initiatives like irrigation safeguard projects and seawater desalination (Moroccan Ministry of Agriculture, n.d.).

In addition to water management, addressing structural land tenure issues was essential to enhance productivity and attract private sector investment. Challenges, including diverse land tenure systems, small-sized farms, limited land registration, and inefficient land consolidation, along with urban expansion that reduced agricultural land availability, have all been a hindrance for progress (Moroccan Ministry of Agriculture, 2015). Thus, to address these issues, the GMP proceeded to acquire 750 000 ha of agricultural land (70 000 ha annually) to make it accessible for private agricultural projects (Mahdi, 2020).

Complementing these efforts, the agricultural value chain was strengthened through targeted investments and aggregation models, connecting upstream production with downstream trade and industry (ADA, n.d). Morocco's diverse, export-oriented value chains – dominated by vegetable and fruit crops like tomatoes, citrus, watermelon, red fruit, argan, dates, and avocado – were bolstered by policies such as subsidies and price regulations under programs like the GMP, the Industrial Acceleration Plan (PAI), and the GGP (Amachraa & MAAD, 2023).

3. Materials and methods

3.1. Study area

3.1.1. Location and character of the agricultural activity

The study was conducted in the Chichaoua sub-basin, which covers an area of approximately 2690 km^2 and is located in the southwestern part of the Tensift basin of Marrakech, in northeastern Morocco (Fig. 2). Within the Tensift basin, agriculture accounts for over 80% of water abstraction, with the Marrakech-Safi region distinguished by its diverse crop production, including olives; citrus; apricots; almonds; vines; apples; walnuts; cereals and vegetables, and contributing to the national agricultural value chains with approximately 25% of the national olive production, 17% of forage production, and 11% of vegetable production (ADA, 2019). Since 2008, agricultural growth has surged, coinciding with the implementation of development strategies. In the Chichaoua sub-basin, agriculture is the main source of income.

Intensive farming is predominant in the upstream part of the plain area, with major land use patterns including arboriculture (mainly olive and citrus trees), market gardening, fodder crops, and cereals. Fig. 2 illustrates the study area within the Tensift basin of Marrakech (Fig. 2-b) and within Morocco (Fig. 2-a), with a detailed view on the Region Of Interest (ROI); presented with a Sentinel-2 Bands Composite (Near Infrared (Band 8), Red (Band 4), Green (Band 3)) image from October 2023 (Fig. 2-c).

The area was selected for study due to its unique distribution of varied impacts of development strategies on land use, both positive and negative. It is divided into two distinct zones (Fig. 2-c): an upstream agricultural plain, 16.90 km long for 26.5 km wide, and a downstream valley along the Chichaoua stream, 29.5 km long for 9.7 km wide. The downstream zone relies on three sources of water: groundwater (pumping), natural springs (mainly Abainou), and on rare occasions, the Chichaoua Wadi, with surface irrigation being the main technique used. In contrast, the upstream area primarily relies on boreholes and has widely adopted drip irrigation. These

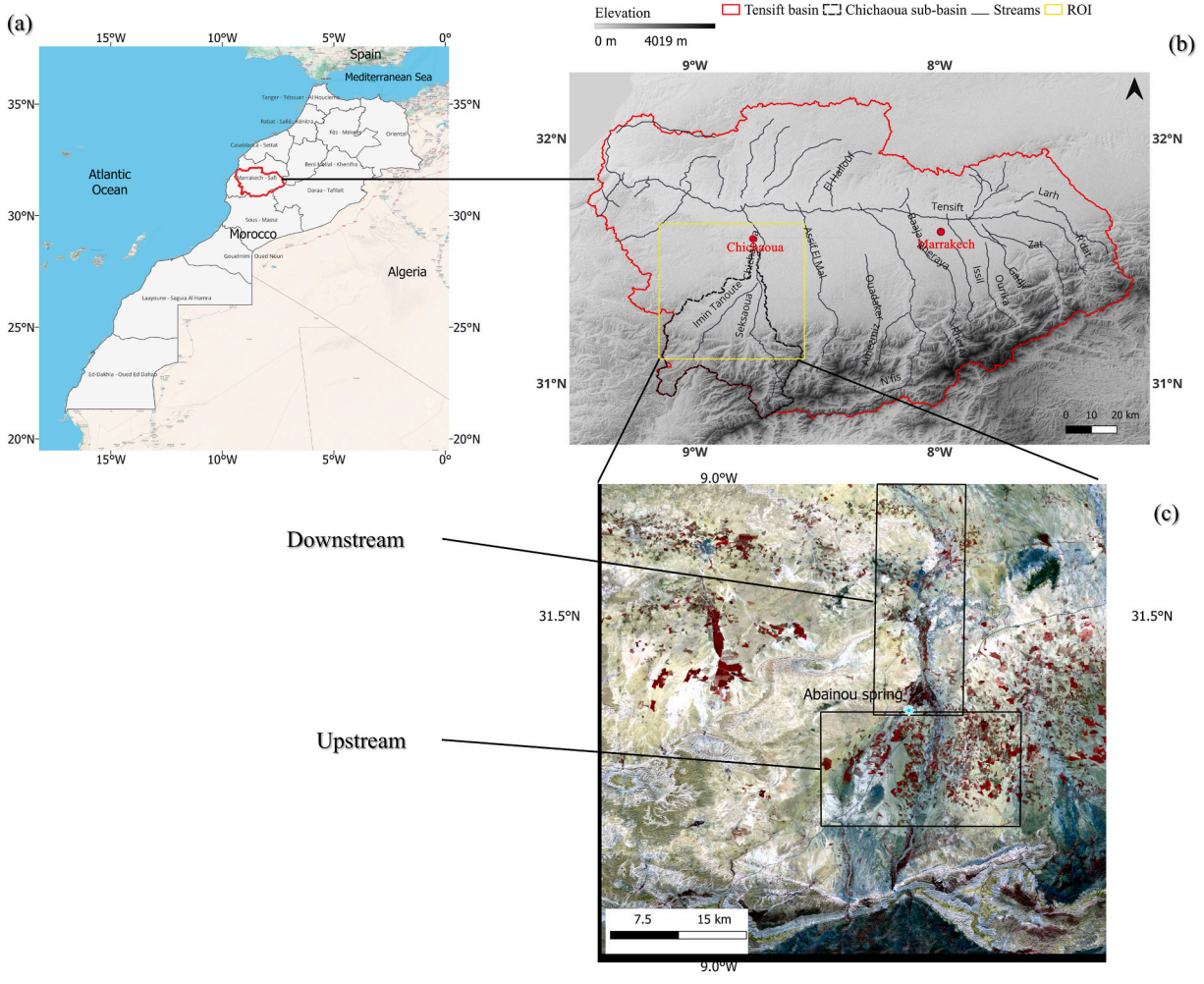

Fig. 2. The location of the Study area in Morocco (a), with the Tensift basin delineation on a DEM (b), and a close-up view of the Region Of Interest (ROI) utilised for the land use classification on the Chichaoua region (c).

zones were differentiated based on their relative position to the region's main natural spring (Abainou Spring). As can be seen on the satellite color composite (Fig. 2-c), the area is mainly occupied by a yellowish color which corresponds to bare soils. Note that generally, the traditional irrigated areas are located in valleys downstream of the modern irrigated plains. The unique spatial distribution of Chichaoua, which mainly depends on natural springs, offers a rare opportunity to study the impact of agricultural development plans in Morocco.

3.1.2. Water resources for irrigation supply

Irrigation for agriculture was historically made by using water streams (the Chichaoua stream in the downstream) and natural springs, while in the upstream area, irrigation is mainly dependent on boreholes. The region is renowned for (one main spring with the highest flow) its natural spring, "Abainou" (this Arabic alliteration is also sometimes written Abeynou, Abaynou or Abeinou), which has historically been the primary irrigation resource for much of the downstream area. However, this spring has experienced a drastic decline in flow, decreasing from over 500 L per second in 1972 (19 Million Cubic Meters per Year) to around 400 L per second in 2010, ultimately drying up entirely (0 L per second) by 2023 (as reported by the Hydraulic Basin Agency of Tensift (ABHT) and confirmed through our local observations in 2023) (Fig. 3). Rainfall in the region is highly variable, fluctuating between a minimum of 100 mm and a maximum of 500 mm annually. Recent years have been particularly marked by recurrent droughts, further exacerbating water scarcity issues. An analysis conducted using ERA5-Land monthly aggregated data (Muñoz-Sabater et al., 2021) summarised at yearly timesteps, highlights the magnitude and frequency of these fluctuations (see Fig. 3).

3.1.3. Land tenure

Land ownership in the Downstream could be categorised into three main types, as reported by the Provincial Directorate of Agriculture (DPA, personal communication): private lands (approximately 80% of the area), state lands (15%), which are classified as collective lands under customary ownership, and collective lands with traditional status (Habous), accounting for the remaining 5%. A survey conducted by the DPA in 2020 revealed that direct land tenure is the dominant form of ownership, with 95% of landowners cultivating their own farms. Leasing is relatively rare, representing only 5% of the total area. A small fraction of the land is managed through shared arrangements. Detailed information on land status specific to the upstream area is unavailable. However, general data covering the entire Chichaoua province (as stated by the local province) – including upstream, downstream, and mountainous areas – provides useful context. The land tenure distribution across the Chichaoua Province, which encompasses the entire Chichaoua sub-basin, is categorised as follows: collective lands (390 000 ha (56.8%)), state lands: (170 000 ha (24.7%)), private lands (101 600 ha (14.8%)), collective lands with traditional status [Habous (2000 ha (0.3%)), Guich (23 000 ha (3.4%))]. In the downstream region, private and collective lands dominate. It can be inferred (according to the provincial data) that private and state lands constitute the majority of landholdings in the upstream area, which could potentially align with the state's broader policy objectives of transforming state and collective lands – historically perceived as obstacles to development – into private farms, as highlighted by Mahdi (2020).

3.2. Dataset

3.2.1. Ground data

Field surveys (open-field observations) were carried out in 2023 using a vehicle transect in the Chichaoua region, to gather essential training data for our analysis, as depicted in Figure A.1 which shows the dates of the field surveys within the satellite acquisition window, while Figure A.2 provides a zoomed-in view of the spatial distribution of the collected data. A total of 375 polygons, spanning a total area of 3412.21 ha, were collected during these surveys. Table 1 summarises the types of crops surveyed and their respective areas. The data collection process involved using the QField mobile application and its integrated GPS capabilities. Post-collection, the

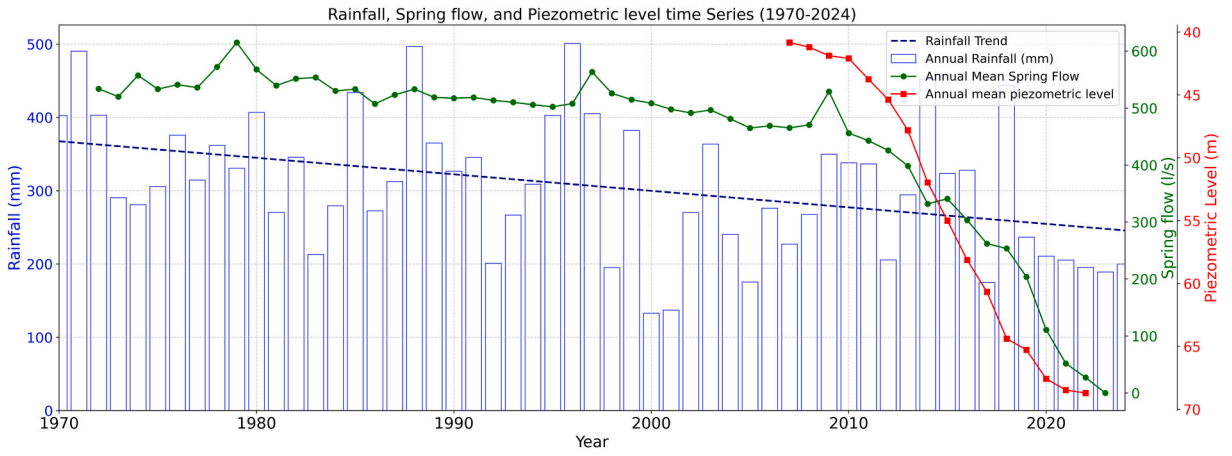

Fig. 3. Historical trends in annual rainfall totals (mm), annual spring flow (l/s) averages, and annual groundwater level (m) averages in the Chichaoua area (1970-2024).

Table 1
The count of polygons and total acreage in hectares (ha) of crops and land cover types acquired during the field surveys in 2023.

Label	Class	Polygons No.	Area (ha)	Remarks
0	Vineyard	5	3.3	Permanent
1	Bare ground	129	3083.8	-
2	Green peas	8	8.0	Season from November to March
3	Olive trees	72	80.0	Permanent, with different intercroppings
4	Double-crop	22	19.4	Generally, onions, green peas, faba beans, and watermelon
5	Alfalfa	30	2.0	-
6	Faba beans	3	1.8	Season from November to March
7	Cereals	6	3.4	Wheat and Barley mainly. Some corn fields were also found.
8	Citrus trees	33	104.2	-
9	Apricot trees	4	8.4	-
10	Watermelon	35	29.6	Season from April to July
11	Water	4	2.1	-
12	Rainfed crops	24	66.2	Only during wet years
	Total	375	3412.2	

polygon geometries and labels were refined using Sentinel-2 RGB composite imagery within the QGIS software.

The data were categorised into 13 distinct classes and subsequently uploaded to the GEE platform as a shapefile asset, with each class assigned a specific numerical label. Various grouping strategies were employed for efficient analysis. For instance, crops like wheat, barley, and maize were combined into a single "Cereals" class. Similarly, fields of onions, green peas, faba beans, and watermelons (during the same year) were merged into a "Double crops" category based on their Normalised Difference Vegetation Index (NDVI) profiles. Additionally, fields classified under the "Water" category were assigned as irrigation basins, with a minimum area threshold of 2500 square meters; set for this classification.

3.2.2. Past tree coverage data

To conduct a basic validation of the historical tree coverage, a total of four historical very high-resolution images (less than 60 cm in Panchromatic band) from Google Earth (GE) were used. Table A.1 summarises these images characteristics. The validation process included the delineation of parcels of trees identified on the GE images as depicted in Figure A.3 which shows the four GE images with these delineations within a polygon inside the ROI, then a superposition of these polygons on the classified maps was conducted right

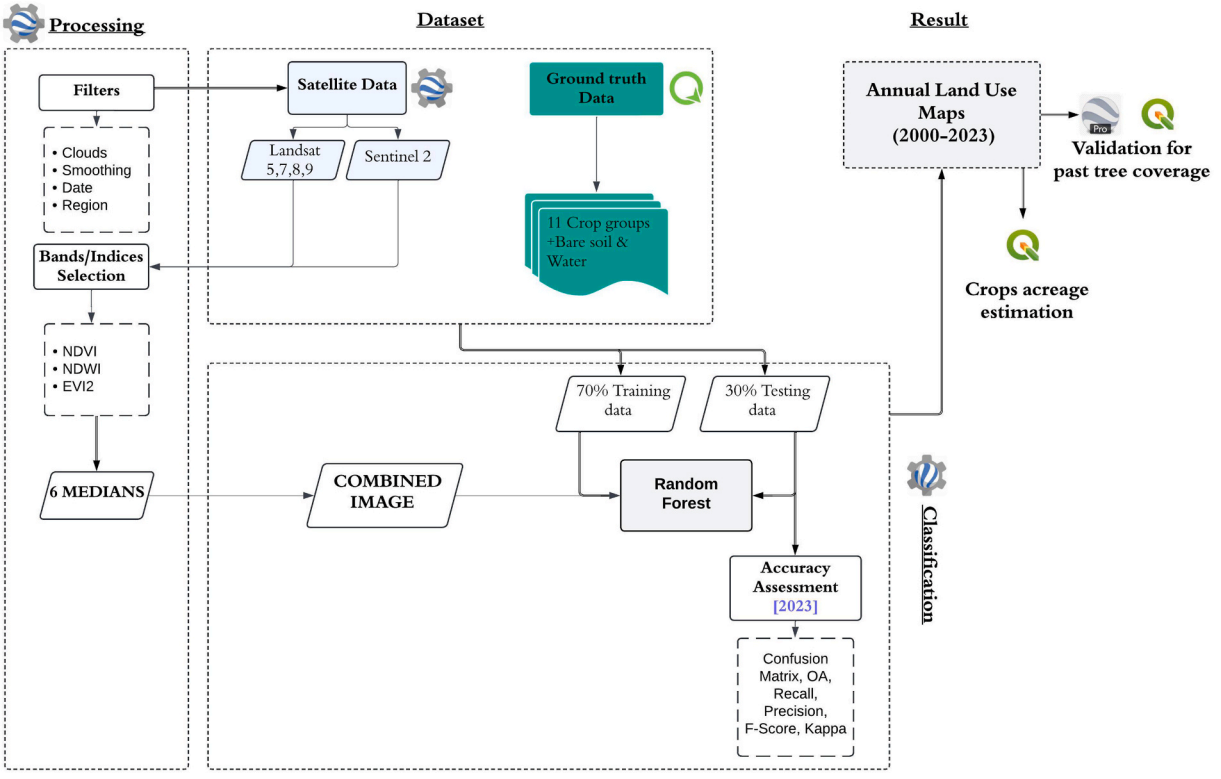

Fig. 4. LULC Classification workflow.

after to analyse similarities, and F-scores were used to evaluate the similarities/precision of the classified fields compared to reality.

3.2.3. Satellite data

A combination of Sentinel-2 (2018-2023) and Landsat satellites 9, 8, 7, and 5 (2001-2017) was utilised for the multi-decadal classification. Data from four specific image tiles were used for each satellite series (IDs Sentinel-2: 29RNQ, 29SNR, 29RMQ, and 29SMR)/(IDs Landsat: Path 202 Row 38, Path 202 Row 39, Path 203 Row 38, and Path 203 Row 39), with the total number of images detailed in Table A.2. Further technical details on the satellite missions and full utilised bands characteristics are provided in Table A.3 and Table A.4 (Appendix A).

3.3. Preprocessing and compositing

The workflow used to produce crop classification maps is summarised in Fig. 4, which presents a step-by-step diagram that includes dataset processing, sampling methods, accuracy assessment, results, and post-processing steps. Key preprocessing steps and RF parameter settings are summarised in Table A.5 (Appendix A). A detailed explanation of each component of the workflow is provided in the following sections.

3.3.1. Data preparation

Landsat and Sentinel-2 satellite data from GEE were used and processed with cloud and smoothing filters to improve quality. Sentinel-2 images were first masked to remove data-lacking edges using the Red-Edge and water vapour bands. A cloud mask was then applied, despite the study area's generally low cloud cover (Marchane et al., 2015); as also demonstrated by the mean annual cloud percentages (Table A.2). Using a 10% cloud cover threshold to define a useable image, 60-88% of Landsat and 62-79% of Sentinel-2 images were cloud-free from 2000 to 2023. The mean annual cloud cover was 4%-21% for Landsat and 12%-22% for Sentinel-2. The Sentinel-2 cloud mask used the "Cloud Probability" dataset, with a 65% probability threshold to classify a pixel as cloud-covered. For Landsat, band names were harmonised across sensors (Roy et al., 2016), and a cloud mask was applied using the Pixel-QA band. A Savitzky-Golay (Savitzky and Golay, 1964) smoothing filter (30-day window, 3rd-degree polynomial) was then used to reduce noise from clouds and atmosphere (Chen et al., 2004). After filtering the datasets, specific bands and indices (like NDVI, EVI2, and NDWI, see Table A.3) were selected for both satellites, choosing Sentinel-2 bands that were spectrally similar to the six Landsat bands used.

To capture seasonal variations for the ML model, a multi-temporal image stack was created by combining median composites from different periods within each year from 2000 to 2023. After several trials, it was found that an interval of 45 days would be a good compromise between the number of available observations and the memory used to make the classification. This interval accounts for sensor-specific revisit cycles – for example, Landsat 8's 16-day revisit frequency ensures 0-3 observations per pixel within each 45-day period. The median of these observations was then computed as suggested by Phan et al. (2020). The process is thus repeated 6 times within each year (see Table A.5 for the periods). The resulting image stack is a multi-band image with each band corresponding to the median composite for a specific time interval. We generated six median composites annually, one median for each period (season). This process produced a composite image with 54 bands (9 bands for each median each period). Annual composites (maps) were privileged because the dominant land-use changes in the region occur on an inter-annual timescale, and the full seasonal cycle dynamics would be disrupted by using finer temporal resolutions.

3.3.2. Classifier setup

The RF classifier is a combined tree-based model. It consists of a collection of tree predictors, where each tree relies on values from a randomly sampled vector distributed independently across all trees in the forest (Breiman, 2001). The aggregation of results from these diverse trees enhances predictive accuracy, leveraging the variation among individual trees for more effective classification (Sujud et al., 2021). It also mitigates overfitting and reduces bias caused by uneven splits in the instance space.

In our study, an RF model was implemented in GEE. A standard stratified sampling (70% training, 30% testing) was used for most classes. This method is common in the literature as it ensures that both sets are representative of the overall class distribution (e.g. (Sujud et al., 2021; Raczko and Zagajewski, 2017),). However, to prevent the model from being biased by the over-represented "bare soil" class and to improve detection of rarer classes, a unique sampling strategy (10% for training, 95% for testing) was justified and applied. This approach was finalised after several trials and visual verification.

The RF classifier has two key parameters: the number of decision trees and variables per split, and it typically exhibits low sensitivity to their specific values (Liaw and Wiener, 2002; Ali et al., 2022). Several studies indicate that RF classification accuracy is not highly impacted by the number of decision trees, provided a sufficiently large number is used (Maxwell et al., 2018). There is no exact threshold for the optimal number of trees beyond which prediction accuracy plateaus. However, it is well-established that accuracy generally improves as the number of trees increases. A number of 100 trees was found to be necessary by Rodriguez-Galiano et al. (2012), while an equilibrium at 50 trees was reported by Ghimire et al. (2012) and Di and Yang (2016). This suggests that the optimal number of trees depends on the specific case (Maxwell et al., 2018).

The classifier in this study was trained with 50 decision trees, and the variables per split was set to the square root of the total by default. After testing various values (20, 50, 70, 100 (not shown)), 50 trees were chosen as the best fit, providing optimal accuracy while minimising computational demands on GEE.

3.3.3. Classifying 2000-2022 images with 2023 data

Since the data collection occurred during 2023, and there was a lack of data for previous years, we trained the RF classifier with

100% of the 2023 data and used the trained model to perform classification for the remaining years (from 1999 to 2022). We created annual composites similar to the 2023 composite. The spectral characteristics were extracted using the 2023 training data.

This application rests on the assumption that the spectral and phenological signatures of the target crop classes remained sufficiently stable over the two-decade study period. While acknowledging potential influences from inter-annual climate variability, long-term agricultural practices, and changes in sensor calibration, we posit that the primary crop types and their seasonal growth patterns in the study region exhibit a certain temporal stability. The use of annual, atmospherically corrected composites mitigates some seasonal and atmospheric noise, and the RF algorithm's robustness to subtle spectral variations further supports this approach. We subsequently produced a series of annual crop maps, which were used to compute crop acreage. This computation was based on a schematic delineation of the valley downstream (area = 68.47 km^2), while the upstream area was defined by the Chichaoua watershed with an altitude limit of 650 m (area = 270.81 km^2). All area calculations were performed using the EPSG:26 191 coordinate reference system.

3.4. Classification accuracy and validation

Classification accuracy was evaluated using a confusion matrix and several statistical metrics (equations summarised in Table A.6): Producer's Accuracy (i.e., Recall), User's Accuracy (i.e., Precision), F-Score, Overall Accuracy (OA), and Cohen's Kappa (Cohen, 1960; Foody, 1992). Accuracy was assessed for both Sentinel-2 and Landsat datasets, with all values expressed as percentages.

The confusion matrix compares classified pixels to ground truth. OA is the proportion of correctly classified pixels. Producer's Accuracy measures the omission error, while User's Accuracy measures commission error (Congalton, 1991).

For previous years, a comprehensive evaluation was limited by lack of historical field data, allowing only the extent of orchards to be assessed. Validation was done by overlaying classified maps with manually delineated tree plots (though specific tree species could not be identified) in QGIS for specific years (Section 3.2.2). Further validation using agricultural census data as an example was impractical due to its coarse spatial and temporal resolution. Unlike in Europe, for example, Moroccan agricultural census records are published only roughly every 20 years (1974, 1996, 2016) at the provincial and prefecture level, with limited public access to finer-scale.

3.5. Transition matrix and markov process

3.5.1. Transition matrix

To study transitions between classification maps, transition matrices were constructed by counting pixel changes between classes. These counts were then normalised to obtain transition probabilities, representing the conditional probability of the system transitioning into a new state, given its current state (Marshall and Randhir, 2008). The probabilities for all map pairs were aggregated into

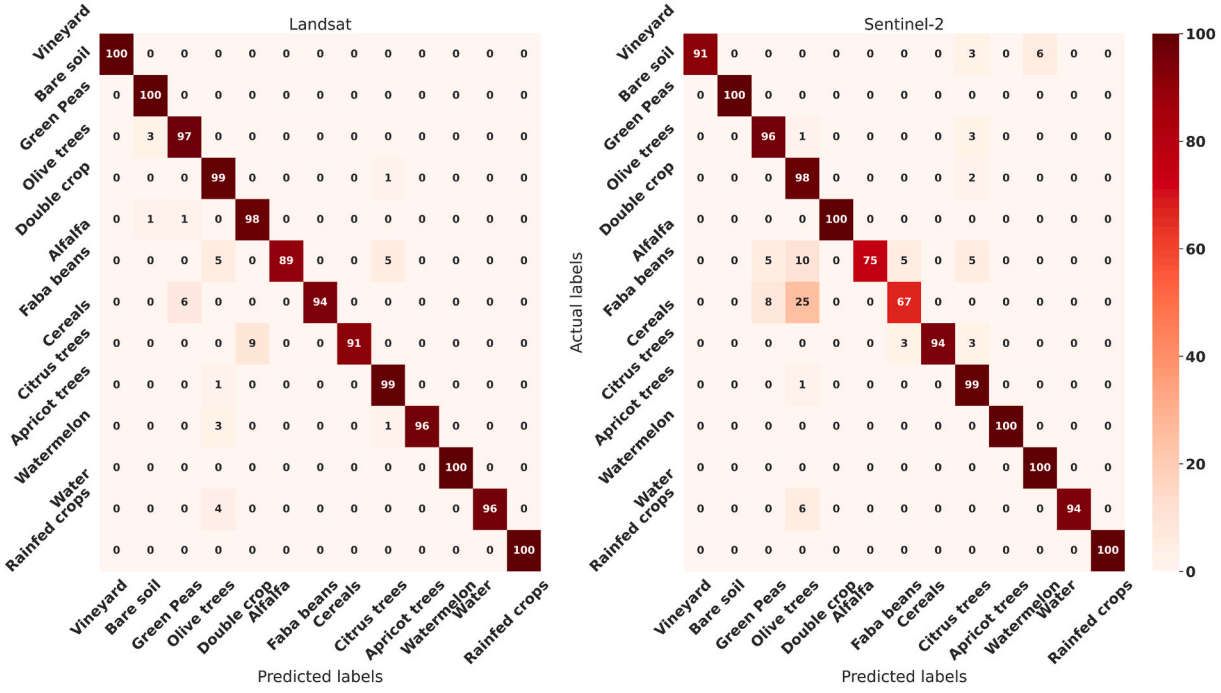

Fig. 5. Confusion matrix for Landsat and Sentinel-2 datasets. Rows represent actual classes; columns represent predicted classes. Values are presented in percentages.

a single transition matrix for the entire 1999 to 2023 period.

3.5.2. Markov chain

The Markov chain is a random process that uses a transition matrix to model the probability of a system transitioning between states over time (Rabta and Aïssani, 2008; Xue, 2001; Sun and Li, 2010). It can simulate a steady state for land cover changes based on the Markovian property, where future states depend solely on the current state, independent of any previous states (Marshall and Randhir, 2008; Gamerman and Lopes, 2014). In this study, the Markov process was used to simulate a stationary state with constant transition probabilities, achieved through repeated matrix multiplication until stability was reached at the 17th iteration. It is important to note that these resulting steady-state distributions represent a conditional projection based on past transition patterns; they do not constitute a forecast of future conditions, which would be influenced by factors such as policy shifts or climate shocks.

3.6. Uncertainty and sensitivity

Errors from previous years (before 2023) can be assessed by examining the likelihood of certain transitions. Transitions considered as "very unlikely" or "not likely" are indicative of implausible changes or potential errors in earlier or later land cover classifications. Examples of such improbable shifts include changes from one tree species to another or from forested areas to water, and vice versa (See Appendix A for indications on the transitions identified as indicative of errors). These unlikely transitions could serve as indicators for reviewing classification errors in past data. The uncertainty or error rate can be estimated by the count of transitions between different tree species or between trees and water, as these are considered to be highly improbable.

4. Results

The results consist of two big sections, Section 4.1, where the land use classification accuracy is being assessed, and Section 4.2, where the land use evolution and trends in the upstream and downstream areas of the study region are being quantified and analysed.

4.1. LULC accuracy assessment and validation

4.1.1. Accuracy assessment for the 2023 classifier

Fig. 5 and Figure A.4 display the accuracy assessments using the Confusion Matrix (i.e., Error Matrix) and its derived analytical metrics: Recall; Precision; and F-Score for each crop class and satellite dataset. Table 3 summarises the OA and Kappa Coefficient values for the 2023 classification for both Sentinel-2 and Landsat data. These metrics were computed using 30% of the test sets described in Section 3.2.1.

OA and Kappa coefficients (Table 3) were around 98% and 99%, demonstrating a high level of classification accuracy. The confusion matrix showed good agreement with the testing set across all classes, although some deviations were noted. For instance, 89% of alfalfa fields were correctly classified by Landsat, with misclassifications with either olive or citrus trees. Similarly, for Sentinel-2, 75% of alfalfa fields were correctly classified, with some misclassified as citrus or olive trees, green peas, or faba beans. For faba beans, Landsat correctly classified 94% of fields, with 6% incorrectly identified as green peas, while Sentinel-2 correctly classified 67% of faba beans fields with misclassifications occurring as green peas (8%) or olive trees (25%). Both Sentinel-2 and Landsat demonstrated close performance in accurately predicting crop classes. The unique cropping practices in the area, where some fields may

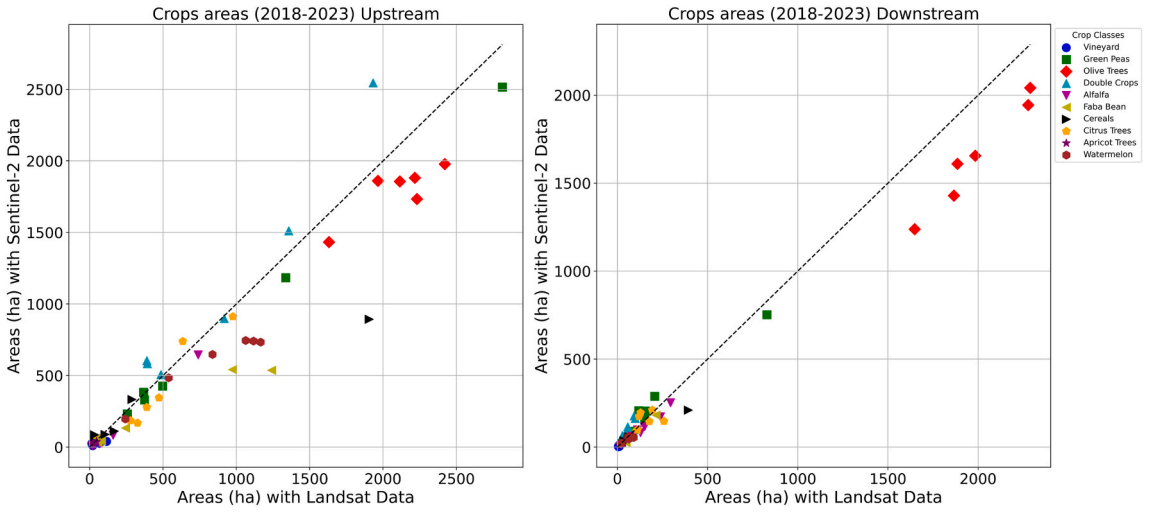

Fig. 6. Comparison of estimated crop areas (hectares) between Sentinel-2 (y-axis) and Landsat (x-axis) for upstream and downstream regions (2018-2023).

contain mixed vegetation, may contribute to these deviations. For instance, some alfalfa fields in the downstream region occasionally include a sparse number of mature olive trees (typically 3-4 per field). This likely explains the observed confusion in the classification error matrix for both Landsat and Sentinel-2. Despite this, other metrics (Recall, Precision, F-score) remained strong overall **(see** Figure A.4). High agreement was observed for most classes, and slightly lower performance for alfalfa and faba beans – partly due to their occasional coexistence with scattered trees like olives; typically, in the downstream area, which can introduce some classification confusion in moderate-resolution imagery.

4.1.2. Satellite dataset consistency comparison

To ensure consistency between Landsat and Sentinel-2 classifications, results of crop areas (upstream and downstream) for the overlapping period from 2018 to 2023 were compared as depicted in Fig. 6 which is a scatterplot of these data. Both datasets produced similar classifications, with a slight overestimation of the olive tree coverage by Landsat. This overestimation was subsequently corrected through a simple linear correction applied to the historical olive tree area estimates derived from Landsat data.

Combining the datasets by extending the time series backward using Landsat data for the 2000-2017 period, while relying on Sentinel-2 data for the 2018-2023 period, had therefore an overall minimal impact on the classification maps (particularly for crop areas). Consequently, prioritising the high spatio-temporal resolution of Sentinel-2 for the more recent period was a practical and acceptable choice.

4.1.3. Assessment of potential errors using transition matrices

Past classification errors can be identified by reviewing pre-2023 data for unlikely transitions. To evaluate the impact of the length of the period used for these transitions on the error percentage, two transition matrices were created: one for annual (year-to-year) transitions and another for transitions spanning four years. Figure A.5 (a) (presents the transition matrix (with values expressed as percentages) for the aggregation of annual transitions for the following periods: 2001-2002, 2002-2003, and 2022-2023. These years were selected based on visual verification of the maps, with only those consecutive years demonstrating accurate classification included. The transitions were calculated using a polygon that encompasses both upstream and downstream areas, as defined in Fig. 2. The estimated error rate for annual transitions was 10.9%, determined by the counts of transitions between different tree species or between trees and water, as these are considered very unlikely. (See Appendix A for indications on the transitions identified as indicative of errors).

Figure A.5 (b) (Appendix A) represents the transition matrix for cumulative transitions over four-year periods: 1999-2003, 2003-2007, 2007-2011, 2011-2016, 2016-2020, and 2020-2023. The estimated error rate for these transitions was 8.7%, calculated using the same transition counts as in Figure A.5 (a). This indicates that analysing transitions over four-year periods – or longer – can reduce errors compared to annual (year-to-year) evaluations, particularly regarding area changes related to crop evolution.

Grouping land use classes into broader categories – 1: Natural (bare soil, water, rainfed crops), 2: Food Crops (alfalfa, faba beans, cereals) which are grown primarily for local consumption, 3: Cash Crops (green peas, double crops, watermelon) which are mainly cultivated for export in this context, and 4: Trees (vineyard, olive, citrus, and apricot trees) – reduced the potential error rate of 0.4%. This analysis considered “very unlikely” transitions only within the upstream region (Table 2), focusing on improbable changes within this area, such as a transition from trees to bare soil. The results emphasize that class grouping reduces classification errors.

4.1.4. Classification validation for past tree coverage (2003, 2010, 2014, 2020)

Since the classification was based on the 2023 training set and applied to images spanning 23 years (from 2000 to 2023), validation for past tree coverage was conducted using GE historical images. As shown in Figure A.6 (Appendix A), the comparison revealed a strong visual alignment between the GE's plots and the LULC maps. Additionally, F-scores and recalls calculated for the comparison years indicated a high level of agreement, with values ranging from 81% to 98%, and error margins ranging from 0.2% to up to 5.5% (Table 3).

4.2. LULC changes from 2000 to 2023: trends and patterns identified

The trends and patterns of the upstream and downstream are explained by the following table and figures: Table A.7 presents the detailed areas per crop class for 2001 and 2023. Fig. 7 presents the annual land use classification maps for years between 2001 and 2023, highlighting the distinction between upstream and downstream regions using polygons. For crop acreage computation, the downstream crop's areas were defined using a schematic delineation of the valley of around 68.47 km^2, whereas the upstream areas were delineated using the Chichaoua watershed with an altitude limit of 650 m; with an area of 270.81 km^2. We expect the proportion of cropland within these delineations to approximate the proportion of irrigated cropland areas served by groundwater, reflecting the typical planting patterns observed in the region. The years (maps) were selected based on their visual accuracy, with those exhibiting minimal interpretive confusion included and those with visual misclassification during high-rainfall years excluded. Fig. 8 provides a summarised illustration of the changes in crop areas over a 23-year period as area graphs, reflecting the impact of two development policies: the GMP and the GGP. Figure A.7 (Appendix A) illustrates the detailed evolution of field acreage as bar plots for all classified crops from 1999 to 2023.

Despite the high classification accuracy obtained in the previous step, some errors and/or confusions can be detected by examining the time series. In particular, it is not logical that the area of olive and citrus trees (downstream) shows such hollows and bumps. The classifications of years like 2003 and 2014 are probably inaccurate due to climatic years (see Fig. 3) very different from the one of 2023 which was used for training the model making, for instance, low vegetation crops and perennial trees having similar temporal

Table 2
Transition matrix of cumulative four-year transitions (1999–2003, 2003–2007, 2007–2011, 2011–2016, 2016–2020, and 2020–2023) over grouped land use classes in the upstream area. Transitions are expressed in percentages. The purple gradient indicates transition percentages from low (light purple) to high (dark purple). Rows indicate the initial land use ("from"), while columns represent the subsequent land use ("to").

		Natural	Food-crops	Cash-crops	Trees
		1	**2**	**3**	**4**
Natural	**1**	91.7	0.6	4.4	3.3
Food-crops	**2**	60.3	12.7	13.6	13.4
Cash-crops	**3**	48.2	2.3	29.1	20.4
Trees	**4**	10.1	1.3	3.3	85.3

Table 3
Overall Accuracy and kappa coefficients for Landsat and Sentinel-2, along with validation accuracy using the F-score and recall for the years 2003, 2010, 2014, and 2020.

	Classification Accuracy		Validation Accuracy			
	Overall Accuracy	Kappa	Years	F-Score	Recall	Confidence intervals
Landsat	0.99	0.98	2003	0.90	0.81	[74.5%, 87.2%]
			2010	0.84	0.72	[66.4%, 77.8%]
			2014	0.99	0.98	[97.7%, 98.9%]
Sentinel-2	0.99	0.99	2020	0.98	0.97	[96.8%, 97.2%]

signatures. However, apart from those years, the trend of each crop seems adequate.

The total irrigated area has more than doubled in the period, growing from 2871 to 6569 (Table A.7). However, the dynamics of the downstream and upstream areas are completely opposite. Over the 23-year period, the total downstream irrigated area decreased by 926 ha (33%), with slight increases for some crops (Watermelon, Double-Crops); while the upstream region has seen an increase of 4624 ha (97%) in irrigated areas. Statistical analysis using the rupture python library (Binary segmentation (BinSeg), cost = radial basis function (rbf), penalty = 1, minimum segmentation length = 3 years) (Truong et al., 2020) identified a rupture occurring in the period 2007-2010 around the 2008 policy period. The exact timing within the 2007-2010 window could not be pinpointed due to missing consecutive annual data points.

To avoid bias from an extreme climatic event, the climatic year 2003 was excluded from the analysis; preliminary tests confirmed that including 2003 distorted the breakpoint detection. As a sensitivity check, we tested the model with and without this data point and found that its inclusion consistently affected the results. For the upstream region, the binary segmentation algorithm detected a break at 2007 when the year 2003 was included. After removing 2003 as a sensitivity check, the algorithm identified a break at 2010 (the first post-policy data point). In the downstream region, binary segmentation detected a break at 2007 with 2003 included, and at 2010 with 2003 excluded. Given the 2008 policy implementation and the first post-policy measurement in 2010, which shows a significant change in the statistical properties of the series (e.g., slope), we adopt 2010 as heuristic break year for comparative trend analysis; for upstream and downstream regions; potentially quantifying a dramatic policy impact. The upstream growth rate accelerated from +79.3 ha/year pre-2010 to +195 ha/year post-2010 (~2.5 times faster), while the downstream decline intensified from −2.2 ha/year pre-2010 to −103.1 ha/year post-2010 (~47.4 times faster).

Downstream, there is a notable decline of around 40% (−653 ha) in olive tree fields. Mann-Kendall (1975) trend analysis confirms this observed decline, showing a statistically significant decrease of −17.81 ha/year ($p = 0.036$, $\tau = -0.515$) for olive trees. In this area, olive trees consist mainly of the traditional Moroccan Picholine variety, widely spaced trees (6 m or more apart), reaching up to 10 m in height. With their deep roots, these trees are drought-resistant but less productive than modern intensive plantations. Alfalfa, a perennial forage crop for livestock (e.g., work animals, sheep, and cows), has decreased by nearly 35%, likely due to a reduction in herd sizes. This decline is statistically validated with a significant trend of −6.52 ha/year ($p = 0.005$, $\tau = -0.697$). This region is also known for pomegranate trees, though they were not distinguishable in the Landsat classification. Regarding seasonal crops, irrigated faba beans and cereals have nearly vanished, with formal trend analysis showing significant declines of −4.35 ha/year ($p = 0.005$, $\tau = -0.636$) for faba beans and −22.82 ha/year ($p = 0.0002$, $\tau = -0.818$) for cereals, while watermelon has seen a modest increase (+1.72 ha/year, $p = 0.012$, $\tau = +0.636$) alongside double cropping (+37 ha). Fig. 7 shows the spatial distribution of changes over eight selected years. The shrinking of the downstream irrigated area is striking. In the first part of the period, the irrigated area contracts

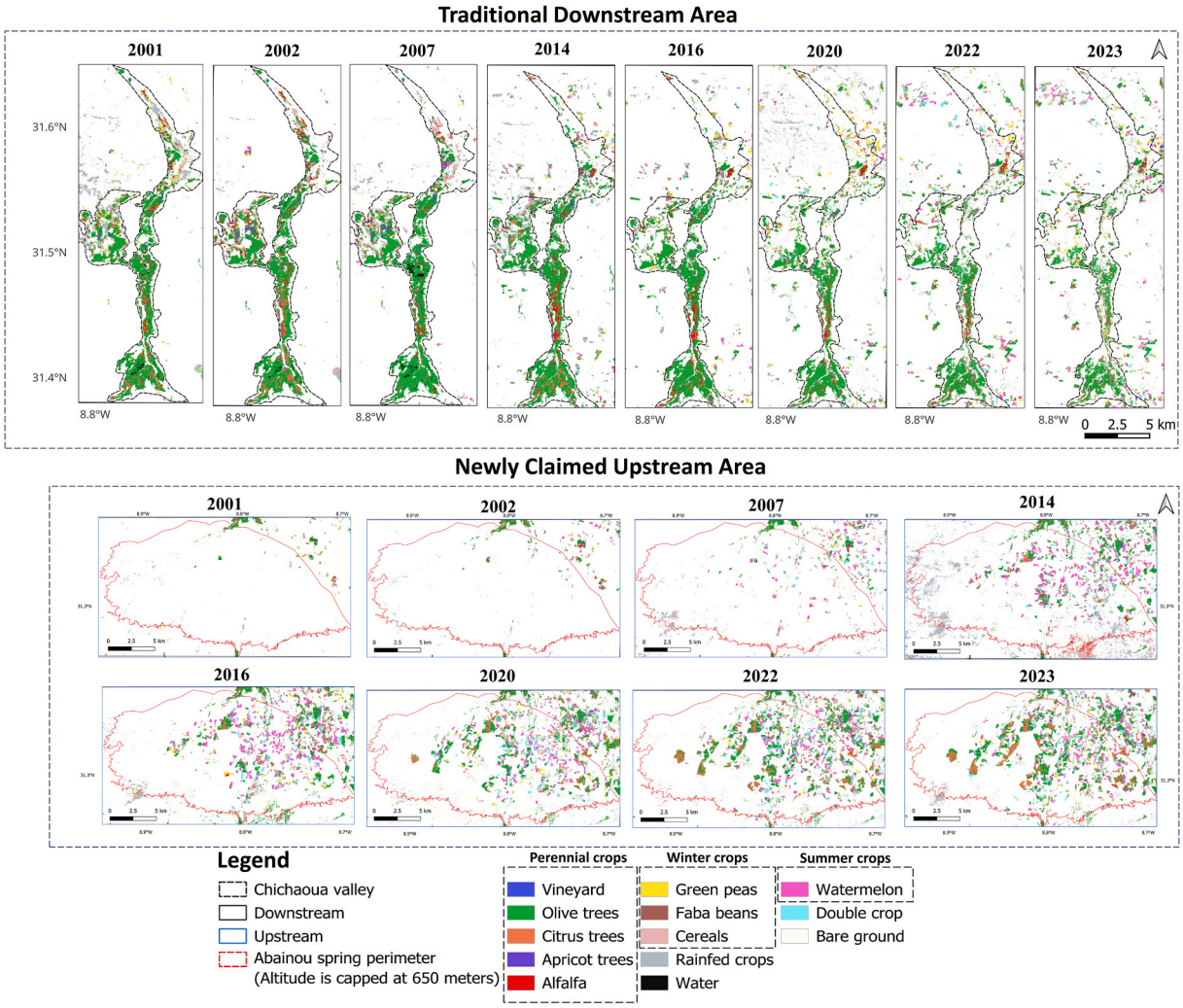

Fig. 7. LULC maps in both downstream and upstream areas illustrating the evolution from 2001 to 2023. Years with minimal interpretive confusion were included; while high-rainfall years were excluded. The top panel represents the Upstream zone (borehole expansion), while the bottom panel represents the Downstream valley (Abainou spring perimeter). Labels and boundaries follow definitions in Section 3.1. (Data: Landsat (30 m) and Sentinel-2 (10 m), USGS/ESA, 2001-2023).

from its northern part, which is more distant from the main wells, suggesting that water availability is a main constraint. In the second decade, the remaining irrigated area becomes even more reduced. The significant reduction in water flow from the primary spring, Abainou, which supplies the area, has mostly impacted the region's irrigated agricultural landscapes. As a summary, along with the spectacular reduction of the irrigated area, it also seems that a redistribution toward cash crops is proceeding, marked by the introduction of seasonal crops such as watermelon and green peas, as well as the practice of double cropping. Meanwhile, subsistence crops like faba beans and cereals are decreasing.

In the Upstream, there was a regional cropland gain from 1999 to 2023, though specific variations occurred due to factors such as rainfall fluctuations and classification errors. Fig. 7 shows that, prior to 2002, only a few irrigated farms were present. By 2007, just before the launch of the GMP, a number of farms – covering a total of 564 ha – were already scattered throughout the area, primarily cultivating seasonal cash crops (watermelon in the summer, green peas in winter, or double cropping). Following the GMP, the prevalence of irrigated crops exploded, beginning with seasonal crops (see the years 2014 and 2016), finally leaving the place to tree crops (see the years 2022 and 2023). Crops such as citrus and olive trees, vineyards, as well as watermelon, green peas, and double-cropping systems, all saw consistent growth over this period. Mann-Kendall trend analysis confirmed statistically significant expansion for most major crops: olive trees showed the strongest growth (+81.76 ha/year, $p = 0.0002$, $\tau = +0.818$), followed by citrus trees (+38.65 ha/year, $p = 0.0002$, $\tau = +0.818$), watermelon (+27.79 ha/year, $p = 0.0005$, $\tau = +0.75$), and double-cropping systems (+21.13 ha/year, $p = 0.005$, $\tau = +0.636$). Additionally, crops like alfalfa, faba beans, and cereals remained relatively stable overall, with some peaks in high-rainfall years. At the end of the period, the total irrigated area went from 100 ha to 4724 ha, which are dominated by olive trees (41%), citrus (22%). Watermelon (15%), green peas (7%) and double crops (11%) are also common.

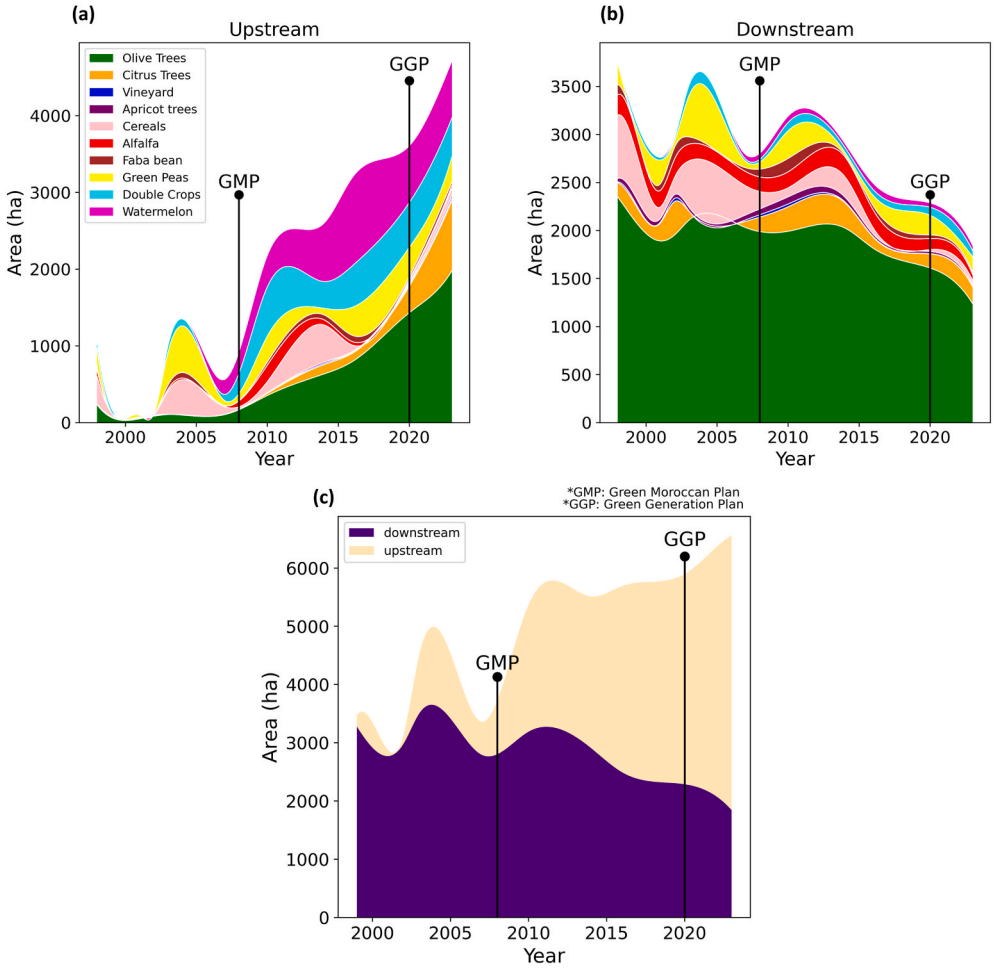

Fig. 8. Irrigated Crop Area (hectares) graphs for both upstream (a) and downstream (b) regions, along with their grouping (c). Areal calculations (in hectares) were performed using an equal-area projection (EPSG:26 191, Merchich Nord Lambert) for the upstream Chichaoua watershed above 650 m (270.81 km^2) and the downstream valley (68.47 km^2). The black lines represent the implementation years of the Green Moroccan Plan (GMP) and the Green Generation Plan (GGP). The peak observed in 2003 is likely a classification error linked to exceptional rainfall. Years with minimal interpretive confusion (1999, 2001, 2002, 2003, 2007, 2010, 2014, 2016, 2020, 2022, 2023) were included, while most high-rainfall years (annual rainfall >300 mm) and non-visually accurate years/maps were excluded from trend calculations. (Data: Landsat (30 m) and Sentinel-2 (10 m), USGS/ESA, 2000-2023).

Table 4
Transition matrix of aggregated 4-year periods for the Upstream area, based on four class groups. Transitions are expressed in percentages.

	Natural	Food-crops	Cash-crops	Trees
Natural	91.7	0.6	4.4	3.3
Food-crops	60.3	12.7	13.6	13.4
Cash-crops	48.2	2.3	29.1	20.4
Trees	10.1	1.3	3.3	85.3

Table 5
Transition matrix of aggregated 4-year periods for the Downstream area, based on four class groups. Transitions are expressed in percentages.

	Natural	Food-crops	Cash-crops	Trees
Natural	91.4	1.0	3.7	3.9
Food-crops	34.7	29.7	10.8	24.8
Cash-crops	68.1	6.4	11.2	14.4
Trees	19.2	3.6	3.7	73.6

4.2.1. *Transformation sequence and stationarity*

4.2.1.1. Transformation matrix. The transformation trends were also analysed using transition matrices (Tables 4 and 5), which were produced by calculating cumulative transitions over four-year periods for data grouped into four classes (Section 4.1.3). The analysis covered the following intervals: 1999–2003, 2003–2007, 2007–2011, 2011–2016, 2016–2020, and 2020–2023. These calculations were conducted separately for both the upstream and downstream areas.

In the downstream region (Table 5), we observed a higher transition rate (19.2%) from trees to bare ground, as also reflected in maps (Fig. 7) and area statistics. In contrast, the upstream region (Table 4) displayed a lower rate for this same transition (10.1%) and higher rates for transitions from bare ground to cash crops (4.4%) and trees (3.3%). Additionally, in the upstream area, a higher transition rate (20.4%) was observed from cash crops to trees, reflecting the common practice of planting young trees alongside other crops, including cash crops.

In the transition matrices diagonals, transition tree-to-tree showed higher percentages, indicating high classification accuracy for tree crops, as these categories remained relatively stable over time. Conversely, lower percentages on the diagonal for cash crops and food crops reflect the dynamic nature of these land use classes, consistent with typical farming practices that involve regular crop rotation and land use changes.

4.2.1.2. Markov chain. The Markov process, or Markov chain, offers insights into how current trends may evolve under the assumption of no external changes. Since land use represents a dynamic, stochastic process, it is generally unrealistic to expect stationarity over long periods. However, land use data may reasonably approximate stationarity if examined over a shorter time span (Bell, 1974).

To determine the stationary state, we used repeated matrix multiplication, multiplying the transition matrix by itself until convergence to a matrix with identical rows (Bell, 1974). This process took 17 steps to reach a stationary state (with each step representing 4 years). The steady-state probabilities for the upstream and downstream regions were as follows (Table 6):

These values indicate the spatial distribution of each class in a stationary state over the 17 steps of iteration using the 4 years transitions. For instance, natural areas, including bare soil, occupy most of the land (69% and 78% for upstream and downstream, respectively), while trees cover significant portions of the regions (24% and 16% for upstream and downstream, respectively). Cash crops occupy 6% and 4% of the upstream and downstream areas, respectively. To gain a clearer understanding of the spatial distribution in terms of surface area, these percentages were converted into hectares (Table 6), based on the total area of the upstream and downstream regions (as detailed in Section 3.1).

By analysing past crop area data grouped into three classes and their stationary state probabilities (Table 6), we could observe the long-term equilibrium patterns of these areas (see Fig. 9), without accounting for dynamic external factors (e.g., climate variability, policy shifts), and interannual variations. It is important to emphasize that this equilibrium represents a conditional projection under the assumption of constant transition probabilities, not a forecast of future land use under potential policy changes or climate shocks. The Markov chain analysis shows system stabilisation occurring after 17 iterations of matrix multiplication.

In the upstream region, tree coverage (which increased significantly between 1999 and 2023) reaches an equilibrium state at 2.2 times its initial probability weight. Cash crops approach equilibrium with a modest growth of about 100 ha in probability weight, while

Table 6
Steady-State probabilities (expressed as percentages and their equivalent area in hectares) for four class groups-Naturals, food crops, cash crops, and trees-in Upstream and Downstream regions, derived using the Markov process.

	Steady-state Probabilities			
	Upstream (%)	Upstream (ha)	Downstream (%)	Downstream (ha)
Naturals	0.69	18685.9	0.78	5340.7
Food Crops	0.01	270.8	0.02	136.9
Cash Crops	0.06	1624.8	0.04	273.8
Trees	0.24	6499.4	0.16	1095.5

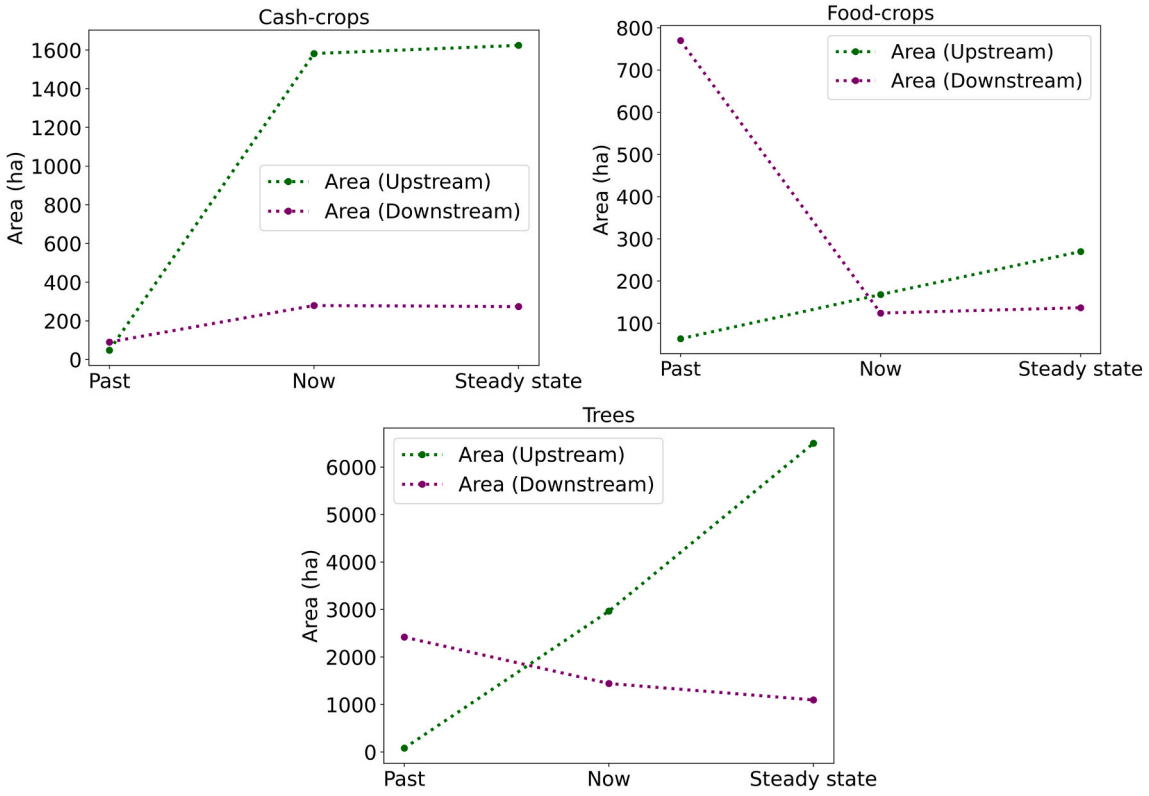

Fig. 9. Crop area (hectares) for upstream (purple line) and downstream (green line) regions, including historical and current periods and the steady-state expected by Markov chain analysis.

food crops stabilise with only marginal changes from their initial state. In the downstream region, tree coverage (which has decreased rapidly from 1999 to 2023) converges at an equilibrium state at 0.75 times its initial probability weight. Cash crops maintain their initial probability weights at equilibrium, while food crops (which also decreased historically) show stable equilibrium probabilities comparable to recent observations.

5. Discussion

The various agricultural action plans that have succeeded one after another in Morocco have fundamentally transformed the landscape, with significant social, economic, and environmental consequences, particularly with the development of new agricultural activities upstream of traditional systems. These policies are linked to the expansion of intensive agriculture with increased irrigated areas, and a shift to higher-value (cash-crop) crops (Faysse, 2015; Molle and Tanouti, 2017). However, this progress was also strongly associated with significant groundwater depletion (Hssaisoune et al., 2020; Ahmed et al., 2021), as farmers often combine drip irrigation techniques with the cultivation of more water-demanding crops, such as vegetables and fruit trees, or adopt practices like denser tree plantations and intercropping (Vecchio, 2018). Additionally, the water savings achieved through drip irrigation are frequently redirected to expand irrigated areas (Benouniche et al., 2014; Kuper et al., 2017), or allocated to alternative uses. This policy has been associated with deepened resource inequities, particularly in regions where small traditional farmers face challenges accessing subsidies or credit due to small land sizes and lack of titles. Wealthier farmers and investors exploit water more efficiently but contribute to its overuse, while smallholders struggle with drying shallow wells and barriers to adopting cost-intensive solutions like deep wells or modern irrigation (Houdret, 2012).

5.1. *Interpretation of upstream and downstream transformation*

The Abainou area of the Chichaoua region, which is the focus of this study, serves as an emblematic example of these upheavals. Indeed, the downstream region was a traditionally irrigated valley where most local farmers are smallholders engaged in subsistence (family) farming, inheriting their farms from previous generations. A diverse range of crops were cultivated, including trees, cereals, forage, and market garden produce. However, yields remain low due to several factors, such as limited rainfall, poor crop management practices, low mechanisation, and labour shortages, as reported by the DPA of the Chichaoua region. Farm sizes downstream are characterised by variability, with small and even micro farms (less than 1 ha) being predominant. The region's agricultural land use has

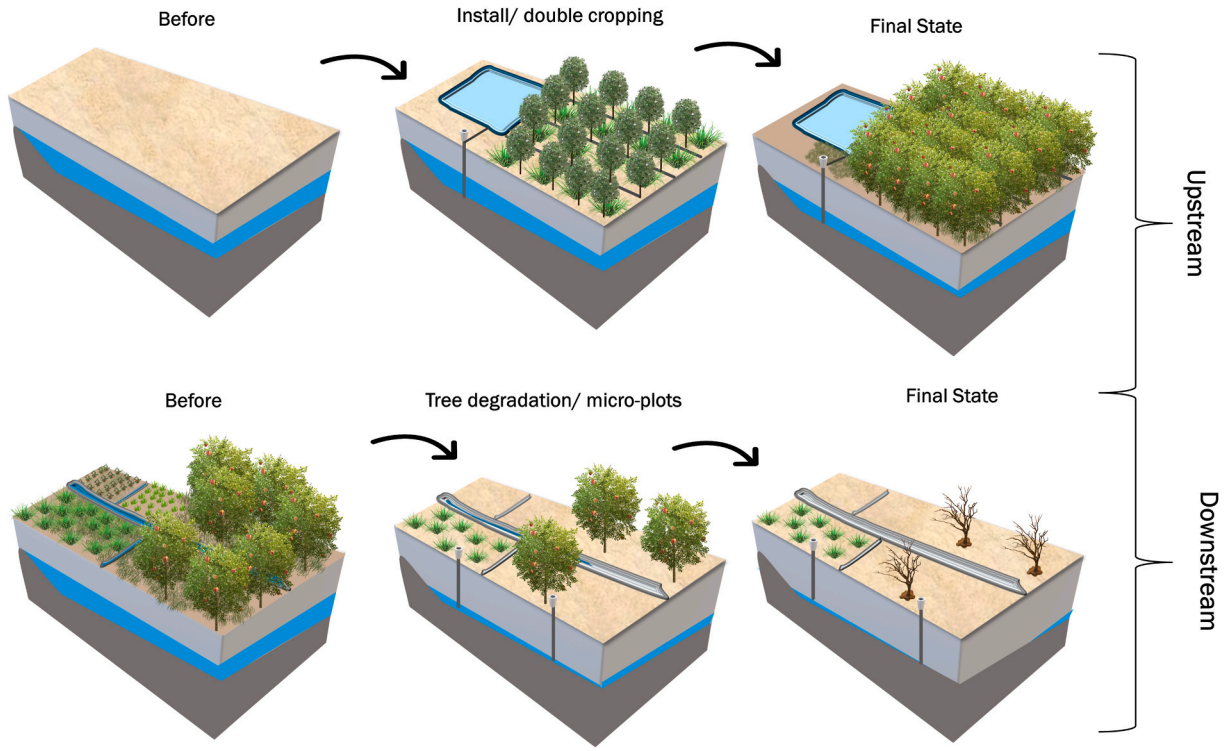

Fig. 10. Schematics representation of the transformation sequence of farmlands in Upstream and Downstream regions in the Chichaoua area, depicting three phases: Initial State (Before the settlement of the GMP), Transitional State (Early transformations following the settlement of the GMP), and Current State (Final Phase).

evolved in distinct phases: in the first phase, which marks the time prior to the establishment of the GMP, the population primarily cultivated trees, mainly olives, along with food crops grown primarily for personal consumption, livestock feed, or sale at local markets. Arboriculture, especially olive trees, was traditionally prominent in this downstream region. In the second phase, which marks the time immediately following the introduction of the GMP, a shift toward abandoning tree lands (referred to as "tree degradation") became evident, especially starting from 2010 (Fig. 10). This period also saw a rise in micro-plotting of food crops (see Figs. 8, 2008-2013), a trend highlighted in the produced land use maps (see Fig. 7). The final state represents the current land use as characterised by recent maps, reflecting conditions nearly 15 years after the establishment of the GMP. This phase highlights a significant reduction in tree coverage and the persistence of minimal agricultural activity, now largely limited to micro-plotting of food crops along with some cash crop cultivation, with a decline in the availability of water resources. These observed changes and trends likely underscore the significant impact of water shortages on croplands.

In stark contrast, the upstream area exemplifies a trajectory of rapid, policy-associated agricultural intensification that is inherently unsustainable, alongside a foundational reliance on groundwater extraction. The upstream area was mainly occupied by bare soil and some sparse private farms. It has undergone a distinct pattern of agricultural development. In the first phase (or the "initial" period), the land was largely bare but possessed favorable natural conditions – such as adequate water availability and soil fertility-; and policy related conditions – such as easy access to land, and subsidies – that supported the establishment and growth of agricultural activity. In the second phase, termed the "installation/double-cropping" phase, agricultural activities intensified with the onset of the GMP. During this period, intensive or large-scale farming practices were introduced. Groundwater pumping and irrigation infrastructure, such as water tanks and pipes, were installed, along with young trees and cash crops. Double-cropping was also adopted, with intercropping practices implemented to optimise land use. This rapid increase of tree orchards was particularly pronounced in the five years following the GMP, as shown in the upstream section of the aggregated area graph (see Fig. 8-c, 2008-2013**).** The final phase, representing the current state, illustrates the full expansion of agricultural activities. Fig. 10 is a schematic representation of these two contrasting scenarios occurring downstream and upstream.

Actually, the GMP was associated with the rapid expansion upstream, marked by easy access and the bypassing restrictions on well drilling in overexploited areas, in conjunction with an expansion of groundwater-based private agriculture (Molle and Tanouti, 2017). Tree orchards have reached productive maturity, which has contributed to a significantly increased water demand. This rising demand is further fuelled by the adoption of intensive and high-density planting systems, including new varieties of olives and citrus trees.

Additionally, summer crops such as watermelon - which can consume up to 6000 m^3/ha annually[1]- strain available water resources, with droughts becoming more frequent and impacting water flow sustainability. Initiatives like the PNEEI (part of the GMP) were aimed at addressing water scarcity by promoting drip irrigation as a means to preserve irrigation water. However, in practice, the emphasis shifted towards extending land equipped with drip irrigation systems rather than ensuring measurable water savings (Benouniche, 2014; Faysse, 2015).

The profound downstream contraction, particularly of olive trees, can probably be explained by the drying of natural springs – like Abainou; the main spring that once provided irrigation water – which can probably be attributed both to the negative trend of precipitation (Fig. 3) and the recent installation of farms upstream. As an observational study, a key challenge is to isolate the impacts of climate variability from anthropogenic factors. The decline of the Abainou spring might primarily be attributed to agricultural intensification upstream post-2007 (see Figs. 7 and 8, 2007-2023). This conclusion is supported by the spring's historical resilience to pre-2007 drought years (see Fig. 3, eg., 2000-2001 and 2005), contrasting with its drastic decline after agricultural expansion, a trend that persisted independently of short-term rainfall patterns. While this interpretation is consistent with the observed spatial and temporal patterns, we note that a definitive attribution would require direct hydrological measurements (such as groundwater level monitoring) to quantify the relative contributions of climate and abstraction.

Thus, while long-term rainfall decrease provides a background stress, the evidence supports the interpretation of groundwater abstraction for irrigation playing a dominant role. These impacts could highlight the unintended consequences of upstream development strategies, where increased water usage has triggered a growing water scarcity crisis, which could, in turn, negatively affect economic activities (like tourism) related to the natural spring.

Upstream, the GMP accompanied a distinct agro-economic model centred on private investment and market-oriented production, which coincided with shifts in the region's social and hydrological dynamics. The GMP was, in fact, an opportunity to facilitate the previous complexities within the land tenure in Morocco. Starting from 2004, the government has undertaken partnerships between public and private sectors, which has provided access to land by private actors (Moroccan and foreign) with adequate financial capital, thus encouraging large-scale and corporate ventures at the expense of smallholder and family farming (Mahdi, 2014, 2020; Mathez and Loftus, 2023). After that, a further access was allowed to investors in 2005 by authorising members of agrarian reform cooperatives to privatise their plot of land and trade it on the land market (Valette et al., 2013; Molle and Tanouti, 2017). Furthermore, the reconversion projects initiated under the GMP coincided with the significant area and dominance of arboriculture in the study zone (Fig. 8 as an example), and the reduction of cereal areas. These projects involved transitioning from rain-fed cereal production to arboriculture. The prevalence of summer crops, such as watermelon, aligns with the objective of cash-crop-oriented agriculture.

As a conclusion, while these strategies have been associated with the expansion of the region's agricultural sector and improvements in productivity, they have also coincided with resource and landscape degradation, as well as social imbalances, particularly in the traditionally irrigated downstream areas. This dual effect underscores the complex trade-offs of development strategies, as noted by Akesbi (2011); Schilling et al. (2012); Faysse (2015); Berdai (2016); and Mathez and Loftus (2023). The stark contrast revealed by our upstream-downstream comparison highlights how a uniform national policy relates to deeply uneven local outcomes.

The diverging patterns we identify – between short-term economic productivity and long-term socio-ecological resilience – mirror a global phenomenon observed across other semi-arid regions, where agricultural intensification and expansion of subsidised, water-intensive export-oriented crops often comes at the cost of resource sustainability. Good examples of these instances are located in India where water-intensive rice and sugarcane was highly subsidised (Sidhu et al., 2020; Chatterjee et al., 2024), in Iran, where unsustainable agricultural practices, like those associated with pistachio production which is geared toward export-linked economic benefits, have led to water overuse and (Nouri et al., 2023), and in Jordan, where subsidised electricity for irrigation pumping has further exacerbated water scarcity (Abu Romman et al., 2024), with similar patterns seen in Saudi Arabia through agricultural expansion supported by interest-free loans and subsidies for water pumping equipment and crop procurement prices, as well as in Yemen through subsidies for well drilling, all raising concerns about long term resource sustainability (Dawoud, 2025). In Australia, for instance, Wheeler et al. (2020) demonstrated that increased subsidies for irrigation infrastructure and expansion, especially for permanent plantings, were a key factor behind a marked growth in water consumption. The tension between economic incentives and environmental limits echoes Morocco's challenges.

5.2. *Assessing land use change in a data scarce context*

To accurately monitor such transformations in data-scarce contexts, this study proposes a methodological framework that uses RF classification with minimal training data. On one hand, the approach aligns with established research on RF's reliability, including its low error rates, high accuracy, minimal parametrization requirements (Belgiu and Drăguţ, 2016; Fang et al., 2020; Talukdar et al., 2020; Sujud et al., 2021). On the other hand, the study demonstrates how model retraining for long term monitoring - leveraging crop spectral signatures with limited ground truth - can overcome sparse datasets, as also shown by Ali et al. (2022) who demonstrated that combining ML with multi-sensor imagery (Sentinel-2 and Landsat 8) and remote sensing indices achieves high accuracy even when using the same training data across both sensors, and by Sujud et al. (2021), who successfully retrained models for 2017 using 2016 data, which supports the viability of temporal transfer. However, the practical implementation for temporal trend analysis requires nuance: local cultivation knowledge and policy interventions must guide plausibility checks to mitigate temporal bias. Additionally,

[1] https://www.cyber-rt.info/life/watermelons-consume-more-water-than-people-in-morocco/.

using years with similar climatic conditions to the training year - and removing visually inaccurate classifications - for trajectory tracing may further reduce the bias, with our error rates (8-10%) affirming the method's viability while addressing this gap for regions lacking high-resolution agricultural census data like Morocco. While this approach shows promise, it would nevertheless be desirable to collect multi-year ground-truth data to further validate and strengthen the methodology. Finally, sensor discrepancies (e.g., between Landsat and Sentinel-2, or between TM/ETM+ and OLI sensors for Landsat) can also pose challenges, though methods like harmonization (Roy et al., 2016) and linear bias correction (applied here for olive tree area estimation) could be employed to reduce inter-sensor variability.

5.3. Limitations and further work

Despite these promising results, several limitations should be considered when interpreting the findings. The study was constrained by the scarcity of multi-year ground-truth data for validation, which is a common challenge in historical land-use analysis, though, the acquisition of high-resolution images facilitated the straightforward interpretation of the tree plots**.** Also, the inter-annual climatic variability may confound the model's performance, as it poses a challenge for transferring the RF model from one year to another. Furthermore, the lack of fine-resolution data - such as detailed land tenure records, agricultural census statistics, and socioeconomic data - combined with a scarcity of plot-level information on equipped areas and subsidies granted - limited our ability to correlate observed land-use changes with specific farm-level practices or socio-economic drivers and to further analyse the quantitative relationship between irrigated areas and public policies.

Some crop classes (e.g., alfalfa, faba beans, green peas) are particularly susceptible to being misclassified. This difficulty in accurate identification (due to misclassification with other spectrally similar classes; or small training samples for these classes) can carry over into estimates of irrigated areas, analysis of land-use changes over time (transition matrices, Markov projections); and trend assessments. As a result, predictions concerning these smaller or spectrally similar crop types are especially uncertain.

While sensor discrepancies (e.g., between Landsat and Sentinel-2) were mitigated using harmonization techniques and linear bias correction, they nonetheless represent a source of uncertainty. Furthermore, the spatio-temporal resolution of older imagery also limits detail; potentially affecting change detection precision for smaller or heterogeneous areas. Cloud coverage could also pose a limitation, particularly in years with very few useable images (e.g., 2003-2006, 2008, 2010-2012, with fewer than 46 images) or in years where over 20% of the available imagery was affected by clouds (e.g., 2004, 2015, 2021). Future research would benefit from the collection of multi-year ground data, the integration of the conventional technique of "photo interpretation of aerial orthophotos'' (Rizzo and Gasparini, 2022) that could be utilised to facilitate the historical reconstruction process, the incorporation of foundational AI models such as DeepMind's AlphaEarth (Brown et al., 2025), and the integration of socio-economic datasets, to enhance classification accuracy, enable the analysis of finer-scale landscape processes, and further strengthen the causal inference of such analyses.

6. Conclusions

This study has quantified 23 years of agricultural land-use changes in Chichaoua, Morocco, by integrating multi-source remote sensing with policy; using a robust classification workflow in GEE. The strength/contribution of this work is threefold: (i) it provides a rare/novel upstream-downstream comparison around a spring system in relation to policy-associated impacts; (ii) it integrates transition-matrix evidence with Markov conditional projections to identify long-term trajectories; and (iii) it offers a reproducible framework for land-use monitoring in data-scarce environments.

The methodological approach achieved high mapping accuracy despite limited historical training data, with overall accuracies of 99%. Validation for the tree crop coverage on the historical maps using GE imagery showed consistent performance across years, with F-scores ranging from 84% to 98%; while transition error analysis revealed stable error rates between 8% (four-year transitions) and 10% (annual transitions), reducible to 0.4% when grouping classes or using longer evaluation periods.

The divergent trajectories between upstream and downstream areas carry critical implications for sustainability and resource management. The dramatic upstream expansion of intensive, groundwater-dependent agriculture, while boosting productivity, has occurred alongside a 40% loss of traditional croplands downstream, leaving a fragmented landscape of smallholder plots. Our Markov Chain analysis, reaching equilibrium after 17 iterations when external factors were held constant, quantified these divergent trajectories: upstream tree coverage stabilises at 2.2 times its initial probability weight, while downstream tree coverage equilibrates at 0.75 times its initial probability weight.

While acknowledging the influence of broader contextual forces such as long-term climate variability and trends to droughts, market dynamics (e.g., market forces incentivising cash-crops), and socio-economic pressures (e.g., shifts like rural migration), our analysis indicates that these general drivers alone cannot explain the stark spatial divergence. Instead, their effects were channeled and most plausibly amplified by the national policy framework and accompanied by human-induced overexploitation of water resources. This interpretation was based on the alignment between the observed irrigation expansion and the timing of successive national development plans, the sharp upstream-downstream contrast in land use trajectories, and the unique transition patterns toward perennial crops.

The findings could offer a clear basis for policy intervention, underscoring that effective decision-making must occur at the regional scale. Sustainable land and water management policies could include monitoring of all water abstraction to control overexploitation. Furthermore, the implementation of major plans must be coupled with supportive policies, such as regulations on groundwater extraction in upstream zones, support for water-efficient practices, and the promotion of diversified livelihoods in downstream areas to enhance resilience.

Several key limitations qualify the interpretation of our findings. While the classification was robust, historical validation is constrained to tree cover extent, not specific tree species. Model performance and transferability may also vary across years due to inter-annual climate variability. The absence of fine-resolution socio-economic data precludes a quantitative link between observed changes and specific policy mechanisms or farm-level decisions. The misclassification of small or spectrally similar crops (e.g., alfalfa, faba beans) can occur due to difficulties in accurate identification, therefore, their predictions are especially uncertain. Furthermore, the harmonization of multi-sensor data; and constraints from older imagery, including cloud contamination and fewer useable scenes, introduce inherent uncertainty into long-term change detection. Finally, projections from the Markov analysis are conditional on constant transition probabilities and should not be interpreted as forecasts under future policy or climate shocks.

Despite these limitations, the method's effectiveness in analysing cropland evolution with a low error rate was not compromised. This paper's insights could provide essential baseline information for future investigations, such as evaluating crop water consumption. Further exploration of the drivers and impacts of these developments could benefit from socio-economic surveys involving local farmers, offering additional insights and validation of the findings. Future research could also benefit from the current findings as a validation dataset to establish a framework for predictive planning using models like Dyna-CLUE **(**dynamic conversion of land use and its effects) (Verburg et al., 1999) and CLUE-s **(**Conversion of Land Use and its Effects at Small region extents) (Herrera-Franco et al., 2022), etc. Furthermore, the workflow algorithm developed in this study is versatile and can be adapted to historical land use analyses in similar regions by simply changing the one-year training set unique to any location, and validating using sample points when available.

CRediT authorship contribution statement

Ikram El Hazdour: Writing – review & editing, Writing – original draft, Visualization, Validation, Software, Methodology, Investigation, Formal analysis, Data curation, Conceptualization. **Michel Le Page:** Writing – review & editing, Supervision, Software, Methodology, Conceptualization. **Lionel Jarlan:** Writing – review & editing, Supervision, Conceptualization. **Marielle Montginoul:** Writing – review & editing, Supervision, Conceptualization. **Lahoucine Hanich:** Writing – review & editing, Supervision, Conceptualization.

Ethical Statement

Hereby, I Ikram EL HAZDOUR consciously assure that for the manuscript “Impact of National Development Policies on Agricultural Land Use Dynamics in Chichaoua, Morocco: A Two-Decade Remote Sensing Analysis” the following is fulfilled:

1) This material is the authors' own original work, which has not been previously published elsewhere.
2) The paper is not currently being considered for publication elsewhere.
3) The paper reflects the authors' own research and analysis in a truthful and complete manner.
4) The paper properly credits the meaningful contributions of co-authors and co-researchers.
5) The results are appropriately placed in the context of prior and existing research.
6) All sources used are properly disclosed (correct citation). Literally copying of text must be indicated as such by using quotation marks and giving proper reference.
7) All authors have been personally and actively involved in substantial work leading to the paper, and will take public responsibility for its content.

The violation of the Ethical Statement rules may result in severe consequences.

To verify compliance with the journal publishing policies, the journal may check the manuscript with their screening tools.

To verify originality, the article may be checked by the originality detection software iThenticate. See alsohttp://www.elsevier.com/editors/plagdetect.

I agree with the above statements and declare that this submission follows the policies of Remote Sensing Applications: Society and Environment as outlined in the Guide for Authors and in the Ethical Statement.

Declaration of competing interest

The authors declare that they have no known competing financial interests or personal relationships that could have appeared to influence the work reported in this paper.

Acknowledgements

This publication was made possible through support provided by the IRD through the ARTS (Allocation de Recherche pour une Thèse de Sud) PhD Grant.

The author would like to thank Mohamed Kasbani (IRD) for his support in data collection during the fieldwork. The fieldwork was carried out with the financial and logistical support of the International Joint Laboratory TREMA (https://www.lmi-trema.ma/). The author would also like to thank the DPA (Provincial Directorate of Agriculture) of the Chichaoua region for their support.

Key Definitions & Abbreviations

RF: Random Forest
OA Overall Accuracy
LULC Land Use/Land Cover
GMP: Green Moroccan Plan
GGP Green Generation Plan
NDVI Normalised Difference Vegetation Index
EVI2 Enhanced Vegetation Index 2
NDWI Normalised Difference Water Index
ML: Machine Learning
GEE Google Earth Engine
GE Google Earth
ROI Region Of Interest
Cash crops: Crops that are mainly cultivated for export in this context
DOY Day Of the Year
Cloud-free For this study, an image was classified as "cloud-free" if less than 10% of its pixels over the study area were identified as cloudy. Cloud pixels were defined using the Sentinel-2 Cloud Probability dataset, with a probability threshold of 65%
Upstream the term refers to the zone within the Chichaoua watershed located upstream of water resources (springs) used for traditional irrigation in the downstream valley. The upstream area spans 16.9 km in length and 26.5 km in width. It is a zone of recent agricultural development, dependent mainly on boreholes for intensive farming
Downstream the term refers to the zone within the Chichaoua watershed, downstream of natural springs, along the Chichaoua valley. The downstream area spans 29.5 km in length and 9.7 km in width. It is a zone of small-scale traditional farming that relies on three sources of water: groundwater (pumping), natural springs (mainly Abainou), and on rare occasions, the Chichaoua wadi, with surface irrigation being the main technique used.

Appendix A. Supplementary data

Supplementary data to this article can be found online at https://doi.org/10.1016/j.rsase.2026.102034.

Data availability

I have shared the link to my code at the Attach file step.
GEE LULC Classification code and dataset (Original data) (Github)

References

Abu Romman, Z., Al-Smadi, B., Weshah, A., 2024. A statistical analysis of the effectiveness of groundwater related policies in mitigating over-extraction in arid regions: challenges and impacts. Groundw. Sustain. Dev. 26, 101203. https://doi.org/10.1016/j.gsd.2024.101203.
ADA. (n.d.). LA STRATEGIE PLAN MAROC VERT. ADA. Retrieved November 16, 2024, from https://www.ada.gov.ma/fr/la-strategie-plan-maroc-vert.
ADA, 2019. Potentialités De La Région De Marrakech-Safi | L'Agence Du Développement Agricole. https://chababagri.ada.gov.ma/fr/potentialites-de-la-region-de-marrakech-safi.
Ahmed, M., Aqnouy, M., Stitou El Messari, J., 2021. Sustainability of Morocco's groundwater resources in response to natural and anthropogenic forces. J. Hydrol. 603, 126866. https://doi.org/10.1016/j.jhydrol.2021.126866.
Akesbi, N., 2011. La nouvelle stratégie agricole du Maroc annonce-t-elle l'insécurité alimentaire du pays. Confluences Méditerranée 78 (3), 93–105. https://doi.org/10.3917/come.078.0093.
Alami Machichi, M., mansouri, loubna E., imani, yasmina, Bourja, O., Lahlou, O., Zennayi, Y., Bourzeix, F., Hanadé Houmma, I., Hadria, R., 2023. Crop mapping using supervised machine learning and deep learning: a systematic literature review. Int. J. Rem. Sens. 44 (8), 2717–2753. https://doi.org/10.1080/01431161.2023.2205984.
Ali, U., Esau, T.J., Farooque, A.A., Zaman, Q.U., Abbas, F., Bilodeau, M.F., 2022. Limiting the collection of ground truth data for land use and land cover maps with machine learning algorithms. ISPRS Int. J. GeoInf. 11 (6), 6. https://doi.org/10.3390/ijgi11060333.
Amachraa, A., Maad, H., 2023. Chaînes globales de valeur tourmentées : risques et opportunités pour L'AGRICULTURE et L'ALIMENTATION. Policy Center for the New South. https://www.policycenter.ma/sites/default/files/2023-02/RP_01-23%20%28Abdelmonim%20AMACHRAA%20%26%20Hassnae%20MAAD%29.pdf.
Belgiu, M., Drăguţ, L., 2016. Random forest in remote sensing: a review of applications and future directions. ISPRS J. Photogrammetry Remote Sens. 114, 24–31. https://doi.org/10.1016/j.isprsjprs.2016.01.011.
Bell, E.J., 1974. Markov analysis of land use change—An application of stochastic processes to remotely sensed data. Soc. Econ. Plann. Sci. 8 (6), 311–316. https://doi.org/10.1016/0038-0121(74)90034-2.
Benouniche, M., 2014. Technical innovation in the making drip irrigation in use in Morocco: actors, bricolages and efficiencies. [Phdthesis, Université Montpellier II - Sciences et Techniques du Languedoc]. https://theses.hal.science/tel-01810938.
Benouniche, M., Kuper, M., Hammani, A., 2014. Mener le goutte à goutte à l'économie d'eau: ambition réaliste ou poursuite d'une chimère? Alternatives Rurales 2.
Berdai, M., 2016. Le Plan Maroc Vert et la sécurité alimentaire: Quelle perspective à l'horizon 2020. New Medit 15 (1), 53–61.
Breiman, L., 2001. Random forests. Mach. Learn. 45 (1), 5–32. https://doi.org/10.1023/A:1010933404324.

Brown, C.F., Kazmierski, M.R., Pasquarella, V.J., Rucklidge, W.J., Samsikova, M., Zhang, C., Shelhamer, E., Lahera, E., Wiles, O., Ilyushchenko, S., Gorelick, N., Zhang, L.L., Alj, S., Schechter, E., Askay, S., Guinan, O., Moore, R., Boukouvalas, A., Kohli, P., 2025. AlphaEarth foundations: an embedding field model for accurate and efficient global mapping from sparse label data. (arXiv:2507.22291). arXiv. https://doi.org/10.48550/arXiv.2507.22291.

Carrasco, L., O'Neil, A.W., Morton, R.D., Rowland, C.S., 2019. Evaluating combinations of temporally aggregated Sentinel-1, Sentinel-2 and landsat 8 for land cover mapping with google Earth engine. Remote Sens. 11 (3). https://doi.org/10.3390/rs11030288. Article 3.

Chatterjee, S., Lamba, R., Zaveri, E.D., 2024. The role of farm subsidies in changing India's water footprint. Nat. Commun. 15 (1). https://doi.org/10.1038/s41467-024-52858-6. Article 1.

Chen, J., Jönsson, Per, Tamura, M., Gu, Z., Matsushita, B., Eklundh, L., 2004. A simple method for reconstructing a high-quality NDVI time-series data set based on the Savitzky–Golay filter. Remote Sensing of Environment 91 (3), 332–344. https://doi.org/10.1016/j.rse.2004.03.014.

Cohen, J., 1960. A coefficient of agreement for nominal scales. Educ. Psychol. Meas. 20 (1), 37–46. https://doi.org/10.1177/001316446002000104.

Congalton, R.G., 1991. A review of assessing the accuracy of classifications of remotely sensed data. Remote Sensing of Environment 37 (1), 35–46. https://doi.org/10.1016/0034-4257(91)90048-B.

Crawford, C.J., Roy, D.P., Arab, S., Barnes, C., Vermote, E., Hulley, G., Gerace, A., Choate, M., Engebretson, C., Micijevic, E., Schmidt, G., Anderson, C., Anderson, M., Bouchard, M., Cook, B., Dittmeier, R., Howard, D., Jenkerson, C., Kim, M., et al., 2023. The 50-year Landsat collection 2 archive. Science of Remote Sensing 8, 100103. https://doi.org/10.1016/j.srs.2023.100103.

Dalin, C., Wada, Y., Kastner, T., Puma, M.J., 2017. Groundwater depletion embedded in international food trade. Nature 543 (7647), 700–704. https://doi.org/10.1038/nature21403.

Das, T., Das, S., 2022. Analysing the role of land use and land cover changes in increasing urban heat phenomenon in Chandannagar city, West Bengal, India. J. Earth Syst. Sci. 131 (4), 261. https://doi.org/10.1007/s12040-022-02010-z.

Das, T., Das, S., 2024. A hydro-geomorphologic assessment of flood generation potentiality in ungauged sub-basins and their prioritization based on traditional, statistical, MCDM and Nash-GIUH models of a tropical plateau-fringe River. J. Hydrol. 640, 131689. https://doi.org/10.1016/j.jhydrol.2024.131689.

Davis, K.F., Dalin, C., DeFries, R., Galloway, J.N., Leach, A.M., Mueller, N.D., 2019. Sustainable pathways for meeting future food demand. In: Ferranti, P., Berry, E. M., Anderson, J.R. (Eds.), Encyclopedia of Food Security and Sustainability. Elsevier, pp. 14–20. https://doi.org/10.1016/B978-0-08-100596-5.21994-X.

Dawoud, M.A., 2025. Groundwater management and governance in MENA Region. In: Ali, S., Negm, A. (Eds.), Groundwater in Developing Countries: Case Studies from MENA, Asia and West Africa. Springer, Nature Switzerland, pp. 67–95. https://doi.org/10.1007/978-3-031-79122-2_3.

Di, Shi, Yang, X., 2016. An assessment of algorithmic parameters affecting image classification accuracy by random forests. Photogramm. Eng. Rem. Sens. 82 (6), 407–417. https://doi.org/10.14358/PERS.82.6.407.

Disperati, L., Virdis, S.G.P., 2015. Assessment of land-use and land-cover changes from 1965 to 2014 in Tam Giang-Cau Hai Lagoon, central Vietnam. Appl. Geogr. 58, 48–64. https://doi.org/10.1016/j.apgeog.2014.12.012.

Elfert, S., Bormann, H., 2010. Simulated impact of past and possible future land use changes on the hydrological response of the Northern German lowland 'Hunte' catchment. J. Hydrol. 383 (3), 245–255. https://doi.org/10.1016/j.jhydrol.2009.12.040.

Famiglietti, J.S., Ferguson, G., 2021. The hidden crisis beneath our feet. Science 372 (6540), 344–345. https://doi.org/10.1126/science.abh2867.

Fang, P., Zhang, X., Wei, P., Wang, Y., Zhang, H., Liu, F., Zhao, J., 2020. The classification performance and mechanism of machine learning algorithms in winter wheat mapping using Sentinel-2 10 m resolution imagery. Applied Sciences 10 (15). https://doi.org/10.3390/app10155075. Article 15.

Faunt, C.C., Sneed, M., Traum, J., Brandt, J.T., 2016. Water availability and land subsidence in the central valley, California, USA. Hydrogeol. J. 24 (3), 675–684. https://doi.org/10.1007/s10040-015-1339-x.

Faysse, N., 2015. The rationale of the green Morocco plan: missing links between goals and implementation. J. N. Afr. Stud. 20 (4), 622–634. https://doi.org/10.1080/13629387.2015.1053112.

Foody, G.M., 1992. On the compensation for chance agreement in image classification accuracy assessment. Remote Sensing Brief. https://www.asprs.org/wp-content/uploads/pers/1992journal/oct/1992_oct_1459-1460.pdf.

Furberg, D., Ban, Y., Nascetti, A., 2019. Monitoring of urbanization and analysis of environmental impact in Stockholm with Sentinel-2A and SPOT-5 multispectral data. Remote Sens. 11 (20). https://doi.org/10.3390/rs11202408. Article 20.

Gamerman, D., Lopes, H.F., 2014. Markov Chain Monte Carlo: Stochastic Simulation for Bayesian Inference, Second Edition, second ed. Chapman and Hall/CRC. https://doi.org/10.1201/9781482296426.

Gebremichael, M., Krishnamurthy, P.K., Ghebremichael, L.T., Alam, S., 2021. What drives crop land use change during multi-year droughts in california's central valley? Prices or concern for water? Remote Sens. 13 (4). https://doi.org/10.3390/rs13040650. Article 4.

Ghimire, B., Rogan, John, Galiano, Víctor Rodríguez, Panday, Prajjwal, Neeti, N., 2012. An evaluation of bagging, boosting, and random forests for land-cover classification in cape cod, Massachusetts, USA. GIScience Remote Sens. 49 (5), 623–643. https://doi.org/10.2747/1548-1603.49.5.623.

Gómez, C., White, J.C., Wulder, M.A., 2016. Optical remotely sensed time series data for land cover classification: a review. ISPRS J. Photogrammetry Remote Sens. 116, 55–72. https://doi.org/10.1016/j.isprsjprs.2016.03.008.

Gorelick, N., Hancher, M., Dixon, M., Ilyushchenko, S., Thau, D., Moore, R., 2017. Google Earth engine: Planetary-scale geospatial analysis for everyone. Remote Sensing of Environment, Big Remotely Sensed Data: Tools, Applications and Experiences 202, 18–27. https://doi.org/10.1016/j.rse.2017.06.031.

Guo, L., Zhao, S., Gao, J., Zhang, H., Zou, Y., Xiao, X., 2022. A novel workflow for crop type mapping with a time series of synthetic aperture radar and optical images in the google Earth engine. Remote Sens. 14 (21). https://doi.org/10.3390/rs14215458. Article 21.

Hermosilla, T., Wulder, M.A., White, J.C., Coops, N.C., 2022. Land cover classification in an era of big and open data: optimizing localized implementation and training data selection to improve mapping outcomes. Remote Sensing of Environment 268, 112780. https://doi.org/10.1016/j.rse.2021.112780.

Herrera-Franco, G., Escandón-Panchana, P., Montalván, F.J., Velastegui-Montoya, A., 2022. CLUE-S model based on GIS applied to management strategies of territory with oil wells—Case study: santa elena, Ecuador. Geogr. Sustain. 3 (4), 366–378. https://doi.org/10.1016/j.geosus.2022.11.001.

Houdret, A., 2012. The water connection: irrigation and politics in southern Morocco, 5 (2).

Hssaisoune, M., Bouchaou, L., Sifeddine, A., Bouimetarhan, I., Chehbouni, A., 2020. Moroccan groundwater resources and evolution with global climate changes. Geosciences 10 (2). https://doi.org/10.3390/geosciences10020081. Article 2.

Irwin, E.G., Geoghegan, J., 2001. Theory, data, methods: developing spatially explicit economic models of land use change. Agriculture, Ecosystems & Environment, Predicting Land-Use Change 85 (1), 7–24. https://doi.org/10.1016/S0167-8809(01)00200-6.

Kanji, S., Das, S., 2025. Exploring the morpho-tectonic nature, hydrological and physical characteristics of a watershed and prioritizing sub-watersheds surface runoff potentialities by integrating MCDM and ensemble machine learning models. J. Environ. Manag. 386, 125772. https://doi.org/10.1016/j.jenvman.2025.125772.

Kelley, L.C., Pitcher, L., Bacon, C., 2018. Using google Earth engine to map complex shade-grown coffee landscapes in Northern Nicaragua. Remote Sens. 10 (6). https://doi.org/10.3390/rs10060952. Article 6.

Kendall, M.G., 1975. Rank Correlation Methods, fourth ed. Griffin.

Kuper, M., Ameur, F., Hammani, A., 2017. Unraveling the enduring paradox of increased pressure on groundwater through efficient drip irrigation. In: Drip Irrigation for Agriculture. Routledge.

Lambert, M.-J., Traoré, P.C.S., Blaes, X., Baret, P., Defourny, P., 2018. Estimating smallholder crops production at village level from Sentinel-2 time series in Mali's cotton belt. Remote Sensing of Environment 216, 647–657. https://doi.org/10.1016/j.rse.2018.06.036.

Lambin, E.F., Geist, H. (Eds.), 2006. Land-Use and Land-Cover Change: Local Processes and Global Impacts. Springer. https://doi.org/10.1007/3-540-32202-7.

Lambin, E.F., Turner, B.L., Geist, H.J., Agbola, S.B., Angelsen, A., Bruce, J.W., Coomes, O.T., Dirzo, R., Fischer, G., Folke, C., George, P.S., Homewood, K., Imbernon, J., Leemans, R., Li, X., Moran, E.F., Mortimore, M., Ramakrishnan, P.S., Richards, J.F., et al., 2001. The causes of land-use and land-cover change: moving beyond the myths. Glob. Environ. Change 11 (4), 261–269. https://doi.org/10.1016/S0959-3780(01)00007-3.

Li, T., López Valencia, O.M., Johansen, K., McCabe, M.F., 2023. A retrospective analysis of national-scale agricultural development in Saudi Arabia from 1990 to 2021. Remote Sens. 15 (3). https://doi.org/10.3390/rs15030731. Article 3.

Liaw, A., Wiener, M., 2002. Classification and Regression by Randomforest, 2.

Liu, J., Hull, V., Batistella, M., DeFries, R., Dietz, T., Fu, F., Hertel, T., Izaurralde, R.C., Lambin, E., Li, S., Martinelli, L., McConnell, W., Moran, E., Naylor, R., Ouyang, Z., Polenske, K., Reenberg, A., de Miranda Rocha, G., Simmons, C., et al., 2013. Framing sustainability in a telecoupled world. Ecol. Soc. 18 (2). https://doi.org/10.5751/ES-05873-180226.

Ma, L., Li, M., Ma, X., Cheng, L., Du, P., Liu, Y., 2017. A review of supervised object-based land-cover image classification. ISPRS J. Photogrammetry Remote Sens. 130, 277–293. https://doi.org/10.1016/j.isprsjprs.2017.06.001.

Mahdi, M., 2014. Devenir du foncier agricole au Maroc. Un cas d'accaparement des terres. New medit: Mediterranean journal of economics, agriculture and environment = Revue méditerranéenne d'economie, agriculture et environment 13 (4), 2–10 (diciembre).

Mahdi, M., 2020. Incidences de l'investissement foncier agricole sur les sociétés rurales A propos de « la classe moyenne agricole. https://doi.org/10.13140/RG.2.2.18482.02245.

Mall, N.K., Herman, J.D., 2019. Water shortage risks from perennial crop expansion in California's central valley. Environ. Res. Lett. 14 (10), 104014. https://doi.org/10.1088/1748-9326/ab4035.

Marchane, A., Jarlan, L., Hanich, L., Boudhar, A., Gascoin, S., Tavernier, A., Filali, N., Le Page, M., Hagolle, O., Berjamy, B., 2015. Assessment of daily MODIS snow cover products to monitor snow cover dynamics over the Moroccan atlas mountain range. Remote Sensing of Environment 160, 72–86. https://doi.org/10.1016/j.rse.2015.01.002.

Marshall, E., Randhir, T.O., 2008. Spatial modeling of land cover change and watershed response using Markovian cellular automata and simulation. Water Resour. Res. 44 (4). https://doi.org/10.1029/2006WR005514.

Mathez, A., Loftus, A., 2023. Endless modernisation: power and knowledge in the green Morocco plan. Environ. Plan. E Nat. Space 6 (1), 87–112. https://doi.org/10.1177/25148486221101541.

Maxwell, A.E., Warner, Timothy A., Fang, F., 2018. Implementation of machine-learning classification in remote sensing: an applied review. Int. J. Rem. Sens. 39 (9), 2784–2817. https://doi.org/10.1080/01431161.2018.1433343.

Molle, F., Tanouti, O., 2017. Squaring the circle: agricultural intensification vs. water conservation in Morocco. Agric. Water Manag. 192, 170–179. https://doi.org/10.1016/j.agwat.2017.07.009.

Moor, A. P. G. de, Calamai, P., with Earth Council, 1997. Subsidizing unsustainable development: undermining the earth with public funds. Earth Council.

Moroccan Ministry of Agriculture. (n.d.). Programmes de maitrise et de gestion de l'eau d'irrigation. Retrieved November 20, 2024, from https://www.agriculture.gov.ma/index.php/en/node/149.

Moroccan Ministry of Agriculture, 2015. Assises Nationales Sur "'La Politique Foncière De L'Etat Et Son Rôle Dans Le Développement Économique Et Social. Maroc.ma. https://www.maroc.ma/fr/actualites/ouverture-skhirat-des-assises-nationales-sur-la-politique-fonciere-de-letat.

Mukherjee, P., Das, T., Das, S., Mazumdar, A., 2024. The green conundrum: navigating the paradox of buffer farmlands of a mangrove forest landscape. Land Use Policy 146, 107305. https://doi.org/10.1016/j.landusepol.2024.107305.

Muñoz-Sabater, J., Dutra, E., Agustí-Panareda, A., Albergel, C., Arduini, G., Balsamo, G., Boussetta, S., Choulga, M., Harrigan, S., Hersbach, H., Martens, B., Miralles, D.G., Piles, M., Rodríguez-Fernández, N.J., Zsoter, E., Buontempo, C., Thépaut, J.-N., 2021. ERA5-Land: a state-of-the-art global reanalysis dataset for land applications. Earth Syst. Sci. Data 13 (9), 4349–4383. https://doi.org/10.5194/essd-13-4349-2021.

Nouri, M., Homaee, M., Pereira, L.S., Bybordi, M., 2023. Water management dilemma in the agricultural sector of Iran: a review focusing on water governance. Agric. Water Manag. 288, 108480. https://doi.org/10.1016/j.agwat.2023.108480.

Ostrom, E., Burger, J., Field, C.B., Norgaard, R.B., Policansky, D., 1999. Revisiting the commons: local lessons, global challenges. Science 284 (5412), 278–282. https://doi.org/10.1126/science.284.5412.278.

Oukaddour, K., Le Page, M., Fakir, Y., 2024. Toward a redefinition of agricultural drought periods—A case study in a mediterranean semi-arid region. Remote Sens. 16 (1). https://doi.org/10.3390/rs16010083. Article 1.

Pal, M., 2005. Random forest classifier for remote sensing classification. Int. J. Rem. Sens. 26 (1), 217–222. https://doi.org/10.1080/01431160412331269698.

Phan, T.N., Kuch, V., Lehnert, L.W., 2020. Land cover classification using google Earth engine and random forest classifier—the role of image composition. Remote Sens. 12 (15). https://doi.org/10.3390/rs12152411. Article 15.

Phiri, D., Morgenroth, J., 2017. Developments in landsat land cover classification methods: a review. Remote Sens. 9 (9). https://doi.org/10.3390/rs9090967. Article 9.

Rabta, B., Aïssani, D., 2008. Strong stability and perturbation bounds for discrete Markov chains. Lin. Algebra Appl. 428 (8), 1921–1927. https://doi.org/10.1016/j.laa.2007.10.036.

Raczko, E., Zagajewski, B., 2017. Comparison of support vector machine, random forest and neural network classifiers for tree species classification on airborne hyperspectral APEX images. European Journal of Remote Sensing (world). https://www.tandfonline.com/doi/abs/10.1080/22797254.2017.1299557.

Rapinel, S., Mony, C., Lecoq, L., Clément, B., Thomas, A., Hubert-Moy, L., 2019. Evaluation of Sentinel-2 time-series for mapping floodplain grassland plant communities. Remote Sensing of Environment 223, 115–129. https://doi.org/10.1016/j.rse.2019.01.018.

Rizzo, M., Gasparini, P., 2022. Land use and land cover photointerpretation. In: Gasparini, P., Di Cosmo, L., Floris, A., De Laurentis, D. (Eds.), Italian National Forest Inventory—Methods and Results of the Third Survey: Inventario Nazionale Delle Foreste E Dei Serbatoi Forestali Di Carbonio—Metodi E Risultati Della Terza Indagine. Springer International Publishing, pp. 49–66. https://doi.org/10.1007/978-3-030-98678-0_3.

Rodell, M., Famiglietti, J.S., Wiese, D.N., Reager, J.T., Beaudoing, H.K., Landerer, F.W., Lo, M.-H., 2018. Emerging trends in global freshwater availability. Nature 557 (7707), 651–659. https://doi.org/10.1038/s41586-018-0123-1.

Rodriguez-Galiano, V.F., Ghimire, B., Rogan, J., Chica-Olmo, M., Rigol-Sanchez, J.P., 2012. An assessment of the effectiveness of a random forest classifier for land-cover classification. ISPRS J. Photogrammetry Remote Sens. 67, 93–104. https://doi.org/10.1016/j.isprsjprs.2011.11.002.

Roy, D.P., Kovalskyy, V., Zhang, H.K., Vermote, E.F., Yan, L., Kumar, S.S., Egorov, A., 2016. Characterization of Landsat-7 to Landsat-8 reflective wavelength and normalized difference vegetation index continuity. Remote Sensing of Environment, Landsat 8 Science Results 185, 57–70. https://doi.org/10.1016/j.rse.2015.12.024.

Roy, D.P., Wulder, M.A., Loveland, T.R., C.e, W., Allen, R.G., Anderson, M.C., Helder, D., Irons, J.R., Johnson, D.M., Kennedy, R., Scambos, T.A., Schaaf, C.B., Schott, J.R., Sheng, Y., Vermote, E.F., Belward, A.S., Bindschadler, R., Cohen, W.B., Gao, F., et al., 2014. Landsat-8: science and product vision for terrestrial global change research. Remote Sensing of Environment 145, 154–172. https://doi.org/10.1016/j.rse.2014.02.001.

Savitzky, Abraham, Golay, M.J.E., 1964. Smoothing and differentiation of data by simplified least squares procedures. Anal. Chem. 36 (8), 1627–1639. https://doi.org/10.1021/ac60214a047.

Scanlon, B.R., Fakhreddine, S., Rateb, A., de Graaf, I., Famiglietti, J., Gleeson, T., Grafton, R.Q., Jobbagy, E., Kebede, S., Kolusu, S.R., Konikow, L.F., Long, D., Mekonnen, M., Schmied, H.M., Mukherjee, A., MacDonald, A., Reedy, R.C., Shamsudduha, M., Simmons, C.T., et al., 2023. Global water resources and the role of groundwater in a resilient water future. Nat. Rev. Earth Environ. 4 (2), 87–101. https://doi.org/10.1038/s43017-022-00378-6.

Schilling, J., Freier, K.P., Hertig, E., Scheffran, J., 2012. Climate change, vulnerability and adaptation in North Africa with focus on Morocco. Agric. Ecosyst. Environ. 156, 12–26. https://doi.org/10.1016/j.agee.2012.04.021.

Shelestov, A., Lavreniuk, M., Kussul, N., Novikov, A., Skakun, S., 2017. Exploring google Earth engine platform for big data processing: classification of multi-temporal satellite imagery for crop mapping. Front. Earth Sci. 5. https://www.frontiersin.org/articles/10.3389/feart.2017.00017.

Sheykhmousa, M., Mahdianpari, M., Ghanbari, H., Mohammadimanesh, F., Ghamisi, P., Homayouni, S., 2020. Support vector machine versus random forest for remote sensing image classification: a meta-analysis and systematic review. IEEE J. Sel. Top. Appl. Earth Obs. Remote Sens. 13, 6308–6325. https://doi.org/10.1109/JSTARS.2020.3026724. IEEE Journal of Selected Topics in Applied Earth Observations and Remote Sensing.

Sidhu, B.S., Kandlikar, M., Ramankutty, N., 2020. Power tariffs for groundwater irrigation in India: a comparative analysis of the environmental, equity, and economic tradeoffs. World Dev. 128, 104836. https://doi.org/10.1016/j.worlddev.2019.104836.

Siebert, S., Burke, J., Faures, J.M., Frenken, K., Hoogeveen, J., Döll, P., Portmann, F.T., 2010. Groundwater use for irrigation – a global inventory. Hydrol. Earth Syst. Sci. 14 (10), 1863–1880. https://doi.org/10.5194/hess-14-1863-2010.

Sujud, L., Jaafar, H., Haj Hassan, M.A., Zurayk, R., 2021. Cannabis detection from optical and RADAR data fusion: a comparative analysis of the SMILE machine learning algorithms in google Earth engine. Remote Sens. Appl.: Soc. Environ. 24, 100639. https://doi.org/10.1016/j.rsase.2021.100639.

Sun, D., Li, X., 2010. Application of markov chain model on environmental fate of phenanthrene in soil and groundwater. In: Procedia Environmental Sciences, International Conference on Ecological Informatics and Ecosystem Conservation (ISEIS 2010), 2, pp. 814–823. https://doi.org/10.1016/j.proenv.2010.10.092.

Talukdar, S., Singha, P., Mahato, S., Shahfahad, Pal, S., Liou, Y.-A., Rahman, A., 2020. Land-use land-cover classification by machine learning classifiers for satellite observations—A review. Remote Sens. 12 (7), 7. https://doi.org/10.3390/rs12071135.

Tayyebi, A., Pijanowski, B.C., Linderman, M., Gratton, C., 2014. Comparing three global parametric and local non-parametric models to simulate land use change in diverse areas of the world. Environ. Model. Software 59, 202–221. https://doi.org/10.1016/j.envsoft.2014.05.022.

Teluguntla, P., Thenkabail, P.S., Oliphant, A., Xiong, J., Gumma, M.K., Congalton, R.G., Yadav, K., Huete, A., 2018. A 30-m landsat-derived cropland extent product of Australia and China using random forest machine learning algorithm on Google Earth Engine cloud computing platform. ISPRS J. Photogrammetry Remote Sens. 144, 325–340. https://doi.org/10.1016/j.isprsjprs.2018.07.017.

Truong, C., Oudre, L., Vayatis, N., 2020. Selective review of offline change point detection methods. Signal Process. 167, 107299. https://doi.org/10.1016/j.sigpro.2019.107299.

Turner, K., Georgiou, S., Clark, R., Brouwer, R., 2004. Economic valuation of water resources in agriculture from the sectoral to a functional perspective of natural resource management. FAO Water Reports). https://www.fao.org/4/y5582e/y5582e04.htm.

Valette, É., Chéry, J.-P., Debolini, M., Azodjilande, J., François, M., Amrani, M.E., 2013. Urbanisation en périphérie de Meknès (Maroc) et devenir des terres agricoles: l'exemple de la coopérative agraire Naïji. Cah. Agric. 22 (6), 6. https://doi.org/10.1684/agr.2013.0656.

Vecchio, K.D., 2018. Has Morocco's groundwater policy changed? Lessons from the institutional approach, 11 (3).

Verburg, P.H., de Koning, G.H.J., Kok, K., Veldkamp, A., Bouma, J., 1999. A spatial explicit allocation procedure for modelling the pattern of land use change based upon actual land use. Ecol. Model. 116 (1), 45–61. https://doi.org/10.1016/S0304-3800(98)00156-2.

Wada, Y., van Beek, L.P.H., Bierkens, M.F.P., 2012. Nonsustainable groundwater sustaining irrigation: a global assessment. Water Resour. Res. 48 (6). https://doi.org/10.1029/2011WR010562.

Wan, B., Guo, Q., Fang, F., Su, Y., Wang, R., 2015. Mapping US urban extents from MODIS data using one-class classification method. Remote Sens. 7 (8). https://doi.org/10.3390/rs70810143. Article 8.

Wang, J.A., Sulla-Menashe, D., Woodcock, C.E., Sonnentag, O., Keeling, R.F., Friedl, M.A., 2020. Extensive land cover change across Arctic–Boreal Northwestern North America from disturbance and climate forcing. Glob. Change Biol. 26 (2), 807–822. https://doi.org/10.1111/gcb.14804.

Wheeler, S.A., Carmody, E., Grafton, R.Q., Kingsford, R.T., Zuo, A., 2020. The rebound effect on water extraction from subsidising irrigation infrastructure in Australia. Resour. Conserv. Recycl. 159, 104755. https://doi.org/10.1016/j.resconrec.2020.104755.

Wulder, M.A., Coops, N.C., Roy, D.P., White, J.C., Hermosilla, T., 2018. Land cover 2.0. Int. J. Rem. Sens. 39 (12), 4254–4284. https://doi.org/10.1080/01431161.2018.1452075.

Wulder, M.A., Masek, J.G., Cohen, W.B., Loveland, T.R., Woodcock, C.E., 2012. Opening the archive: how free data has enabled the science and monitoring promise of Landsat. Remote Sensing of Environment, Landsat Legacy Special Issue 122, 2–10. https://doi.org/10.1016/j.rse.2012.01.010.

Xin, Q., Olofsson, P., Zhu, Z., Tan, B., Woodcock, C.E., 2013. Toward near real-time monitoring of forest disturbance by fusion of MODIS and Landsat data. Remote Sensing of Environment 135, 234–247. https://doi.org/10.1016/j.rse.2013.04.002.

Xue, J., 2001. Blockwise perturbation theory for nearly uncoupled Markov chains and its application. Lin. Algebra Appl. 326 (1), 173–191. https://doi.org/10.1016/S0024-3795(00)00280-9.

Yang, C., Huang, Q., Li, Z., Liu, K., Hu, F., 2017. Big data and cloud computing: innovation opportunities and challenges. Int. J. Digit. Earth 10 (1), 13–53. https://doi.org/10.1080/17538947.2016.1239771.

Zhao, J., Zhong, Y., Hu, X., Wei, L., Zhang, L., 2020. A robust spectral-spatial approach to identifying heterogeneous crops using remote sensing imagery with high spectral and spatial resolutions. Remote Sensing of Environment 239, 111605. https://doi.org/10.1016/j.rse.2019.111605.